



OPEN

Imidazo[1,2-c]quinazolines as a novel and potent scaffold of α -glucosidase inhibitors: design, synthesis, biological evaluations, and in silico studies

Fariba Peytam¹, Faezeh sadat Hosseini², Malak Hekmati², Bahareh Bayati³, Mahdis Sadeghi Moghadam³, Zahra Emamgholipour³, Loghman Firoozpour³, Somayeh Mojtavavi⁴, Mohammad Ali Faramarzi⁴, Seyed Esmaeil Sadat-Ebrahimi³, Maliheh Barazandeh Tehrani³ & Alireza Foroumadi^{1,3}✉

α -Glucosidase inhibition is an approved treatment for type 2 diabetes mellitus (T2DM). In an attempt to develop novel anti- α -glucosidase agents, two series of substituted imidazo[1,2-c]quinazolines, namely 6a–c and 11a–o, were synthesized using a simple, straightforward synthetic routes. These compounds were thoroughly characterized by IR, ¹H and ¹³C NMR spectroscopy, as well as mass spectrometry and elemental analysis. Subsequently, the inhibitory activities of these compounds were evaluated against *Saccharomyces cerevisiae* α -glucosidase. In present study, acarbose was utilized as a positive control. These imidazoquinazolines exhibited excellent to great inhibitory potencies with IC₅₀ values ranging from 12.44 ± 0.38 μ M to 308.33 ± 0.06 μ M, which were several times more potent than standard drug with IC₅₀ value of 750.0 ± 1.5 μ M. Representatively, compound 11j showed remarkable anti- α -glucosidase potency with IC₅₀ = 12.44 ± 0.38 μ M, which was 60.3 times more potent than positive control acarbose. To explore the potential inhibition mechanism, further evaluations including kinetic analysis, circular dichroism, fluorescence spectroscopy, and thermodynamic profile were carried out for the most potent compound 11j. Moreover, molecular docking studies and in silico ADME prediction for all imidazoquinazolines 6a–c and 11a–o were performed to reveal their important binding interactions, as well as their physicochemical and drug-likeness properties, respectively.

Diabetes mellitus (DM), mainly characterized as inadequate control of blood levels of glucose, has emerged as a remarkable health challenges over recent decades. Statics reveals that the rate of diabetes occurrence around the world was 536.6 million people in 2021, and this figure is predicted to reach 783.2 million people by 2045¹. Diabetes is categorized into several subtypes with various etiologies, presentations, and treatments. Moreover, this chronic disease caused various health problems including cardiovascular diseases, hypertension, obesity, kidney diseases, and blindness. Consequently, a huge financial burden on the global health system has been imposed by this illness². Considering the alarming rate of diabetes as well as complicated, severe issues associated with it, extensive efforts have already been made to manage this disease.

Diabetes mellitus is classified into several groups, including type 1, type 2, maturity-onset diabetes of the young (MODY), gestational diabetes, neonatal diabetes, and steroid-induced diabetes. Notably, the main subtypes are type 1 diabetes mellitus (T1DM) and type 2 diabetes mellitus (T2DM)³. These two subtypes have different pathophysiology, presentation, and management strategies. T1DM is characterized by defective insulin secretion, while T2DM involves an impaired response to insulin. However, they have a potential for hyperglycemia

¹Drug Design and Development Research Center, The Institute of Pharmaceutical Sciences (TIPS), Tehran University of Medical Sciences, Tehran, Iran. ²Department of Organic Chemistry, Faculty of Pharmaceutical Chemistry, Tehran Medical Sciences, Islamic Azad University, Tehran, Iran. ³Department of Medicinal Chemistry, Faculty of Pharmacy, Tehran University of Medical Sciences, Tehran, Iran. ⁴Department of Pharmaceutical Biotechnology, Faculty of Pharmacy, Tehran University of Medical Sciences, Tehran, Iran. ✉email: aforoumadi@yahoo.com

in common. Genetic background for both types is critical as a risk factor, but T1DM tends to occur in children, whereas T2DM is prevalent among middle-aged and older adults due to prolonged hyperglycemia resulting from their poor lifestyle and dietary choices. Statistics indicate that 1 in 11 adults suffers from diabetes mellitus, and 90% of patients have T2DM. Given this high prevalence, extensive research is currently being conducted to effectively manage this particular subtype^{4,5}.

Since T2DM is mainly identified by a high level of glucose in blood (hyperglycemia), one of the pivotal strategies to control this disease is to interfere with the digestion of dietary carbohydrates. α -Glucosidase is an enzyme located in the brush border of the small intestine, and its role is the hydrolysis of this long chain sugar to monosaccharide units, which are subsequently released to the bloodstream. Therefore, one approved approach for the treatment of T2DM and its resultant postprandial hyperglycemia is the inhibition of α -glucosidase to slow down glucose absorption, thereby reducing postprandial glucose blood concentrations. Currently, there are three commercial drugs to control T2DM through the α -glucosidase inhibitory mechanism: acarbose, voglibose, and miglitol, among which acarbose is the most widely used and studied drug^{6,7}.

A complex oligosaccharide, acarbose, competitively and reversibly binds to the oligosaccharide site of α -glucosidase in small intestine in a dose-dependent manner. This binding prevents the breakdown of disaccharide and oligosaccharide substrates into absorbable monosaccharides. Despite the efficacy of acarbose as an α -glucosidase inhibitor, it causes several undesirable side effects for patients, the most noticeable of which are diarrhea, abdominal discomfort, as well as bloating and flatulence⁸. Therefore, a great deal of effort over recent decade has been made to discover and develop more potent α -glucosidase inhibitors having improved safety and pharmacological profiles to replace acarbose. To this aim, numerous heterocyclic α -glucosidase inhibitors have been reported. Among them, two valuable nitrogen-containing pharmacophores, various functionalized quinazolines^{9–24} and imidazoles^{25–34} have exhibited great inhibitory potencies compared to acarbose as the standard drug. Figure 1 summarizes some structures and IC₅₀ values of the most active compounds from these studies. Therefore, considering the proved potency of these pharmacophores, providing novel imidazole-quinazoline analog with the hope of finding further potent α -glucosidase inhibitors could be an interesting research topic in medicinal chemistry.

One well-established strategy for designing further novel and potent compounds is the hybridization of two scaffolds which have demonstrated promising inhibitory potencies. Various compounds bearing substituted quinazolines and imidazoles as potential α -glucosidase inhibitors have been already reported separately. However, there is limited investigation into the inhibitory activity of compounds containing both of these heterocycles. For example, Fig. 2 shows compounds M and N as the most potent derivatives from these studies, which were synthesized and evaluated against α -glucosidase, possessing noticeable inhibition in comparison with acarbose. Another strategy involves fusing two heterocycles to provide imidazoquinazoline backbone. Among several isomers of this skeleton, imidazo[1,2-*c*]quinazoline was selected for the present study. This scaffold has displayed anticancer³⁵, antitubercular³⁶, antifungal³⁷, antimicrobial and antioxidant^{38–40} activities; however, its α -glucosidase inhibitory potency has yet to be explored. Therefore, this biological evaluation could be a fascinating study in medicinal chemistry (Fig. 2).

As part of our ongoing research to find potential α -glucosidase inhibitors^{41–48}, imidazo[1,2-*c*]quinazoline was introduced as a novel inhibitor backbone in present study. To this aim, two facile, efficient synthetic protocols were employed to obtain substituted benzo[4,5]imidazo[1,2-*c*]quinazoline 6 and poly-substituted imidazo[1,2-*c*]quinazolines 11 and evaluate their in vitro potencies in comparison with acarbose as the standard drug. These compounds exhibited excellent to remarkable inhibitory activity. Subsequently, further assessments, including

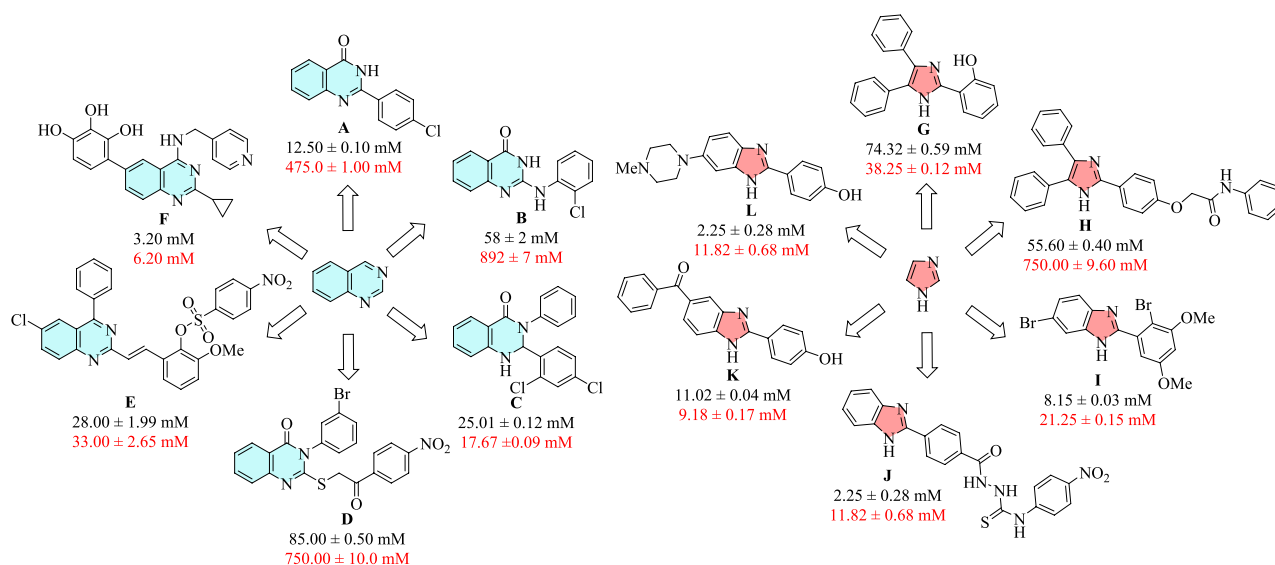


Figure 1. α -Glucosidase inhibitors bearing substituted quinazolines A–F and substituted imidazoles G–L. The IC₅₀ values are written in black for inhibitors and red for acarbose.

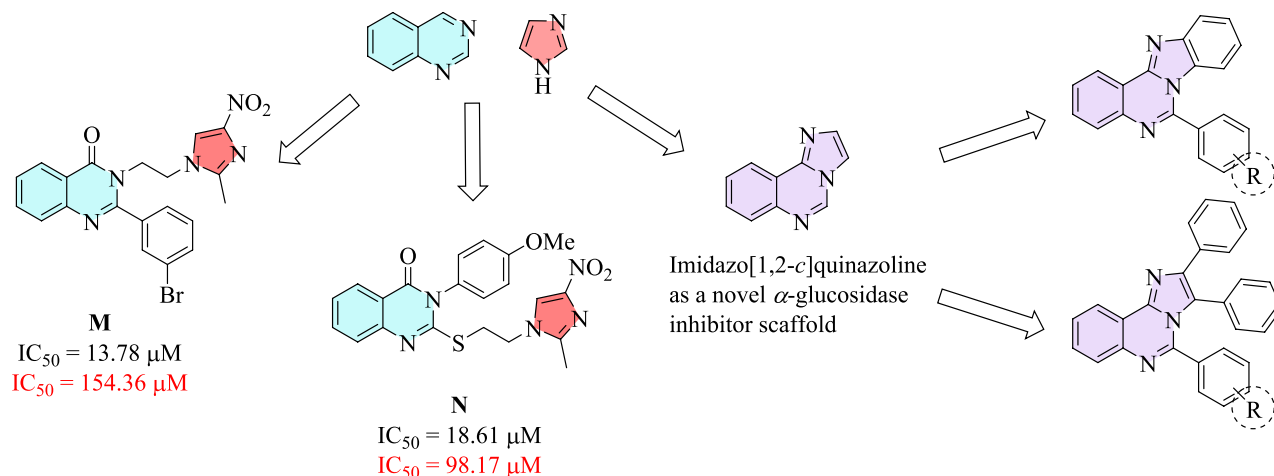


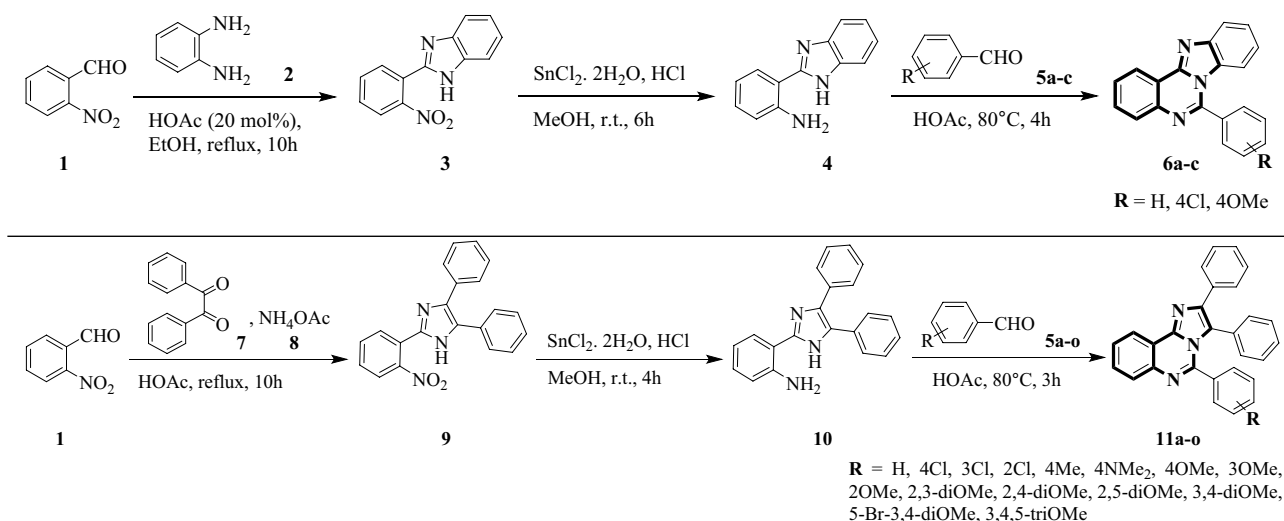
Figure 2. Design strategy toward two series substituted imidazo[1,2-*c*]quinazolines. The IC_{50} values are written in black for inhibitors and red for acarbose.

kinetic study, circular dichroism measurement, fluorescence quenching measurements, and thermodynamic analysis of binding to α -glucosidase were carried out for the most active compound **11j**. Finally, computational investigations, including molecular docking and in silico ADME studies were performed for imidazoquinazolines **6** and **11** to investigate the mode of their interactions with the active site of α -glucosidase and predict the compounds' druglike properties, respectively.

Results and discussion

Chemistry. In present study, simple and efficient synthetic routes toward two series of substituted imidazoquinazolines **6** and **11** were performed. As illustrated in Scheme 1, the first step to obtain benzo[4,5]imidazo[1,2-*c*]quinazoline **6** was a cyclization reaction between 2-nitrobenzaldehyde **1** and benzene-1,2-diamine **2**. This reaction occurred in the presence of catalytic amount of glacial acetic acid in ethanol under the reflux conditions to afford 2-(2-Nitrophenyl)-1*H*-benzo[*d*]imidazole **3**. On the other hand, the protocol to obtain highly-substituted imidazo[1,2-*c*]quinazolines **11** was initiated through a cyclization reaction between 2-nitrobenzaldehyde **1**, benzil **7**, and ammonium acetate **8** under the reflux conditions in glacial acetic acid to produce 2-(2-Nitrophenyl)-4,5-diphenyl-1*H*-imidazole **9**. Subsequent steps in the synthesis were shared for both scaffolds.

The nitro functionality in compounds **3** and **9** went through the reduction reaction using stannous chloride dihydrate ($SnCl_2 \cdot 2H_2O$) and hydrochloric acid in methanol to afford the amine moiety **4** and **10**. Finally, a condensation-cyclization reaction between these adducts and substituted benzaldehydes **5** in glacial acetic acid at 80 °C occurred to obtain corresponding substituted imidazo[1,2-*c*]quinazolines **6a-c** and **11a-o** in great to excellent yields. The structures of the isolated compounds **3**, **4**, **6a-c**, **9**, **10**, and **11a-o** were deduced on the basis of their IR, 1H and ^{13}C NMR spectroscopy, as well as mass spectrometry and elemental analysis. Partial assignments of these resonances are given in the Experimental Part.



Scheme 1. Synthesis of substituted imidazo[1,2-*c*]quinazolines **6a-c** and **11a-o**.

In vitro α -glucosidase inhibitory activity. The target substituted imidazo[1,2-*c*]quinazolines **6a–c** and **11a–o** were evaluated for their in vitro *Saccharomyces cerevisiae* α -glucosidase inhibitory activities to investigate the role of substituents on the imidazole moiety and the phenyl ring originated from benzaldehyde moieties. In this study, acarbose was utilized as a positive control. The obtained results were summarized in Tables 1 and 2. Our studies were initiated through the synthesis of derivatives **6a–c** as well as **11a**, **11b**, and **11g** to evaluate their potencies and reveal the role of substituents on the imidazole ring. Compounds from second series exhibited superior inhibitory activities in comparison with their analogues from the first series; therefore, we followed our studies by the synthesis and investigation of other 5-(substituted aryl)-2,3-diphenylimidazo[1,2-*c*]quinazolines **11c–f**, **h–o**.

As illustrated in Table 2, imidazoquinazolines **11** demonstrated good to excellent α -glucosidase inhibitory potencies, ranging from $12.44 \pm 0.38 \mu\text{M}$ to $273.28 \pm 0.09 \mu\text{M}$, in comparison with acarbose ($\text{IC}_{50} = 750.0 \pm 1.5 \mu\text{M}$). The correlations between their structures and observed activities are explained comprehensively below:

To initiate, an unsubstituted phenyl ring showed moderate inhibitory potency (compound **11a**, $\text{IC}_{50} = 209.15 \pm 0.04 \mu\text{M}$). Introducing a chlorine atom as an electron-withdrawing group at any position (compounds **11b**, **11c**, and **11d**) caused a detrimental effect on the α -glucosidase inhibitory potencies. However, replacing this atom with electron-donating groups including methyl (Me), *N,N*-dimethyl ($\text{N}(\text{Me})_2$), and methoxy (OMe) at C-4 position improved the inhibitory activity noticeably (compounds **11e**, **11f**, and **11g**), among which **11g** exhibited better results ($\text{IC}_{50} = 82.64 \pm 0.03 \mu\text{M}$). This led us to investigate the role of this substituent at other position of phenyl ring or the presence of additional OMe group. With this in mind, other compounds were synthesized for further evaluation. Moving the OMe from C-4 to C-3 and 2 enhanced the inhibitory activity against α -glucosidase (compound **11h** with $\text{IC}_{50} = 47.92 \pm 0.18 \mu\text{M}$ and **11i** with $\text{IC}_{50} = 24.25 \pm 0.13 \mu\text{M}$).

Considering the constructive role of OMe on the phenyl ring, particularly at C-2 position, additional OMe group was introduced. This strategy led to synthesis of two valuable compounds, namely **11j** and **11k**, which emerged as the most potent derivatives among all the synthesized imidazoquinazolines. Compound **11j** bearing two OMe groups at C-2 and 3 exhibited remarkable inhibitory potency against α -glucosidase ($\text{IC}_{50} = 12.44 \pm 0.38 \mu\text{M}$), which was 60.3 times more potent than standard inhibitor ($\text{IC}_{50} = 750.0 \pm 1.5 \mu\text{M}$). Furthermore, compound **11k** with two OMe groups at C-2 and 4 ranked as the second most potent compound in this series ($\text{IC}_{50} = 14.32 \pm 0.05 \mu\text{M}$). Additionally, the presence of this group at C-3 and 4 showed excellent inhibitory activity (compound **11m** with $\text{IC}_{50} = 21.57 \pm 0.32 \mu\text{M}$).

Among the compounds bearing two Ome groups, **11l** showed comparatively less potency, which might be related to the deteriorative effect of C-5 position. This inference could be confirmed by comparing the results of compounds **11n** ($\text{IC}_{50} = 46.73 \pm 0.07 \mu\text{M}$) and **11o** ($\text{IC}_{50} = 154.88 \pm 0.36 \mu\text{M}$) with **11m** ($\text{IC}_{50} = 21.57 \pm 0.32 \mu\text{M}$). It revealed that the presence of any substituent at C-5 position, whether electron-donating group like OMe or electron-withdrawing group like bromine, results in a moderate decrease in α -glucosidase inhibitory activity. Moreover, bromine as an electron-withdrawing group caused a detrimental effect on the inhibitory activity, which is in great agreement with earlier results in compounds **11b–d**.

A statistical analysis using the T-test was performed for both series **6a–c** and **11a–o**. All compounds indicated a significant statistical difference ($p < 0.001$) between the IC_{50} values of each compound in comparison with acarbose as standard drug.

Comparing the IC_{50} values of benzo[4,5]imidazo[1,2-*c*]quinazolines **6** with their corresponding analogs from 5-(substituted aryl)-2,3-diphenylimidazo[1,2-*c*]quinazolines **11** revealed the notable influence of substituents on the imidazole moiety on the α -glucosidase inhibitory activity, as the presence of two phenyl rings on this core improved the potency. Moreover, the aforementioned SAR analysis showed that electron-donating group, particularly OMe, improved the α -glucosidase inhibitory potency, while electron-withdrawing group like chlorine or bromine caused a noticeable detrimental inhibition effect. In conclusion, imidazoquinazolines bearing two OMe groups, particularly when positioned at C-2 and 3 as seen in compound **11j**, exhibited substantial inhibitory activities. Finally, compound **11j** emerged as the most potent derivative having remarkable activity against α -glucosidase. Consequently, it was chosen for further evaluations.

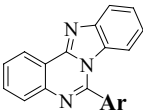
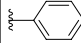
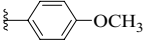
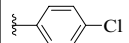
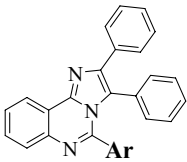
					
Label	Ar	IC_{50} (μM)	Label	Ar	IC_{50} (μM)
6a		256.48 ± 0.14^b	6c		124.28 ± 0.37^b
6b		308.33 ± 0.06^b	Acarbose		750.0 ± 1.5

Table 1. Substrate scope and in vitro α -glucosidase inhibitory activity of compounds **6a–c**. ^aValues are the mean \pm SD. All experiments were performed at least three times. ^bp Value for all compounds was less than 0.001 in comparison with standard drug acarbose.



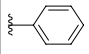
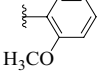
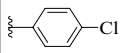
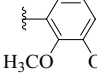
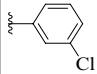
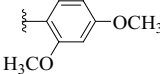
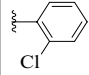
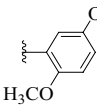
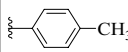
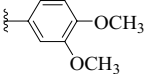
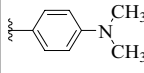
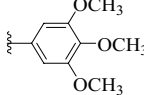
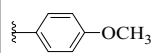
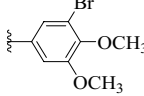
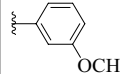
Label	Ar	IC ₅₀ (μM) ± SD	Label	Ar	IC ₅₀ (μM) ± SD
11a		209.15 ± 0.04 ^b	11i		24.25 ± 0.13 ^b
11b		273.28 ± 0.09 ^b	11j		12.44 ± 0.38 ^b
11c		246.49 ± 0.18 ^b	11k		14.32 ± 0.05 ^b
11d		253.08 ± 0.26 ^b	11l		64.29 ± 0.54 ^b
11e		124.47 ± 0.29 ^b	11m		21.57 ± 0.32 ^b
11f		168.36 ± 0.15 ^b	11n		46.73 ± 0.07 ^b
11g		82.64 ± 0.03 ^b	11o		154.88 ± 0.36 ^b
11h		47.92 ± 0.18 ^b			
Acarbose		750.0 ± 1.5	Acarbose		750.0 ± 1.5

Table 2. Substrate scope and in vitro α -glucosidase inhibitory activity of compounds **11a–o**. ^aValues are the mean \pm SD. All experiments were performed at least three times. ^bp value for all compounds was less than 0.05 in comparison with standard drug acarbose.

Enzyme kinetic study. The enzyme kinetic study was performed to reveal the inhibition mode of imidazoquinazoline **11j**. There are two enzyme kinetic constants: Michaelis constant (K_m) and maximum velocity of the reaction (V_{max}) which are calculated using initial velocity measurements at different inhibitors concentrations (for example, 0, 3.1, 6.2, and 12.4 μ M in present study). As illustrated in Fig. 3A, the Lineweaver–Burk plot exhibited the K_m value increased with increasing concentration of compound **11j**, while V_{max} did not change. The results indicated that this imidazoquinazoline bonded to the active site on the enzyme and competes with the substrate for binding to this region, indicating a competitive type of inhibition. Moreover, the plot of the K_m versus different concentrations of inhibitor gave an estimate of the inhibition constant as K_i value of 11.0 μ M (Fig. 3B).

Circular dichroism spectroscopy. The difference between the absorption of right and left circularly polarized light is measured in circular dichroism spectroscopy (CD) in order to reveal the chiral environment around amino acid residues. The CD spectrum in the far ultraviolet region ranged from 190 to 240 nm is mainly used to provide valuable information about the arrangement of protein bonds and secondary structure of the proteins in dilute solutions. There are several principal conformations like α -helix, extended β structure (or β -sheet), β -turn, and random coil (which are unordered structures). They are characterized as follow: α -helix structures by negative CD bands at 222 and 208 nm and a positive CD band at approximately 190 nm; β -sheet structures by a negative CD band in the region of 210–220 nm; β -turn structures by a negative CD band between 180 and 190 nm; and the spectra of random coil by a characteristic negative CD band in region of 200 nm^{49,50}.

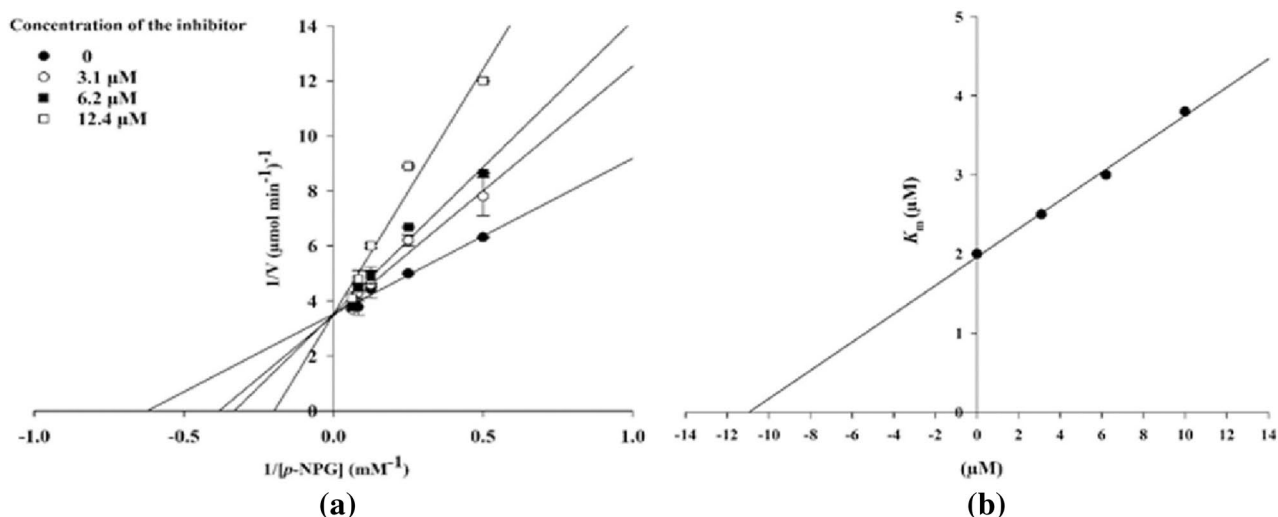


Figure 3. Kinetics of α -glucosidase inhibition by sample **11j**: (A) the Lineweaver–Burk plot in the absence and presence of different concentrations of sample **11j**; (B) the secondary plot between K_m and various concentrations of sample **11j**.

To study the impact of imidazo[1,2-*c*]quinazoline **11j** on the secondary structure of α -glucosidase (Fig. 4b), the CD spectra (180–250 nm) was measured and analyzed using the CDNN software to be compared with the native enzyme (Fig. 4a). The percent of observed conformations are summarized in Table 3. As it can be seen, our inhibitor increased noticeably the figures for α -helix and β -turn; while random coils removed; therefore, this imidazo[1,2-*c*]quinazoline **11j** can determine the conformation of the enzyme and fix chiral side chains in orientations. Moreover, this compound can change the secondary structure of α -glucosidase, resulting to inhibit its performance.

Fluorescence spectroscopy measurements. Fluorescence spectroscopy assay is a frequently used method to investigate the potential interactions between inhibitors and enzymes under physiological conditions, because binding of inhibitors changes the fluorescence characteristics and tertiary structure of the protein.

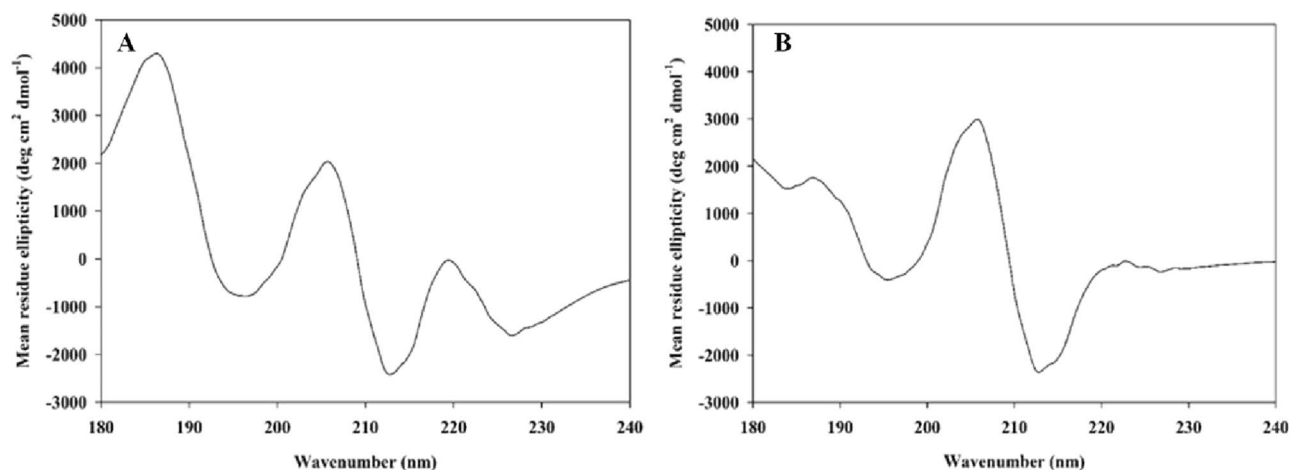


Figure 4. Circular dichroism (CD) spectra of the α -glucosidase: (A) in the absence of inhibitor (control); (B) in the presence of imidazoquinazoline **11j**.

Inhibitor	α -Helix (%)	β -Turn (%)	Random coil (%)
Control ^a	28.8	28.8	42.4
Imidazoquinazoline 11j ^b	50.3	49.7	0

Table 3. The secondary structure content of α -glucosidase. ^aControl is native enzyme in the absence of an inhibitor. ^bThe concentration of imidazoquinazoline **11j** was 12.4 μM .

Moreover, it can predict the tertiary structure of the enzyme and provide more accurate information about the binding constant, number of binding sites, and thermodynamic parameters of the studied interactions.

In present study, fluorescence spectroscopy measurement was performed between imidazo[1,2-*c*]quinazoline **11j** and the active site of enzyme using a Synergy HTX multi-mode reader (Biotek Instruments, Winooski, VT, USA) equipped with a quartz cuvette of 10 mm. The excitation wavelength was 280 nm, and the emission spectra were reported at five different temperatures in the range from 300 to 450 nm with 10 accumulations for each collection point. The emission spectrum was adjusted for the background fluorescence from the buffer solution and for the inner filter effect promoted by the inhibitors (Fig. 5).

The results obtained from this evaluation revealed that the fluorescence intensity of α -glucosidase increased to 340 nm and subsequently decreased (the λ_{\max} was 340 nm). On the other hand, there are three amino acids—tryptophan, tyrosine, and phenylalanine—that play a role in the enzyme's intrinsic fluorescence property, referred to as fluorophores. Among them, the maximum intensity of tryptophan at 280 nm is about 340 nm; therefore, imidazo[1,2-*c*]quinazoline **11j** must be located proximity to the tryptophan residues within the α -glucosidase binding site when this inhibitor bound to the enzyme and changed the tertiary structure of the enzyme.

There are two types of fluorescence quenching: dynamic and static. Dynamic quenching arises from the collisional encounter between the fluorophore (tryptophan residues) and the quencher (inhibitor). Conversely, static quenching results from the formation a ground-state complex between fluorophore and quencher. Results revealed that the combination of fluorophores (tryptophan residues) and quencher (imidazo[1,2-*c*]quinazoline **11j**) exhibited a static quenching mechanism. Therefore, the binding parameters can be determined as follow:

The reaction is determined as $P + D \rightarrow D_nP$ in which P is the protein, D is the drug molecule (inhibitor), and D_nP is the new complex molecule. The binding constant for this complex for this complex, denoted as K_A , is calculated using Eq. (1). In the static quenching mechanism, the number of binding sites, which is named “n”, remains constant. Since the number of the binding site of protein and drug is n and 1, respectively, the equivalent concentration of the complex D_nP is $n[D_nP]$. Moreover, the equivalent concentration of the protein is $n[P]$, and the equivalent concentration of the drug is [D]:

$$K_A = \frac{n[D_nP]}{[D]n[P]} \quad (1)$$

The total concentration of protein is $[P_t]$, and the total concentration of the drug is $[D_t]$; therefore, $[P_f] = [P_t] + [D_nP]$ and $[D_f] = [D_t] - n[D_nP]$. Since protein (P) is the only fluorescence in present study, thus:

$$\frac{F_0}{F} = \frac{[P_t]}{[P_f]} \quad (2)$$

F and F_0 are the fluorescence intensity of protein in the presence and absence of inhibitor, respectively. Therefore, the relationship between the fluorescence intensity and the total concentration of the drug could be deduced:

$$\frac{F_0}{F} = \frac{K_A [D_t] F_0}{(F_0 - F) - n K_A [P_t]} \quad (3)$$

As the total concentration of protein was kept at a constant value (at 46 nM), while the total concentration of the drug was changed. Using the Eq. (3), a plot of F_0/F Vs. $[D_t]$ $F_0/(F_0 - F)$ was obtained, as depicted in Fig. 6. K_A , n, and r at 20 °C can also be calculated, as listed in Table 4:

Thermodynamic analysis of binding of imidazoquinazoline **11j to α -glucosidase.** This fluorescent intensity data was plotted as a function of temperature and binding constants; therefore, thermodynamic

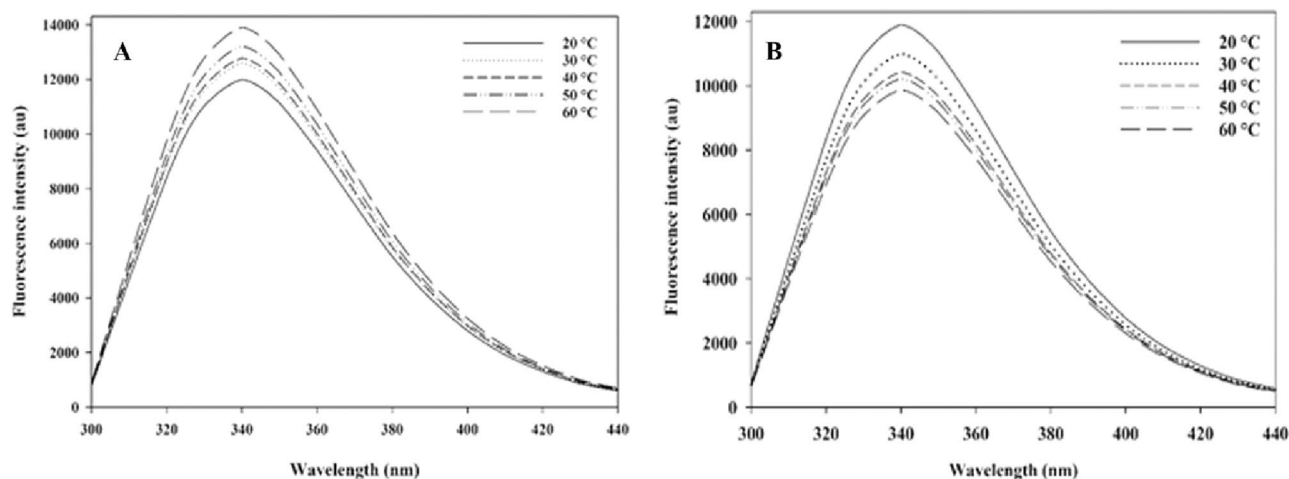


Figure 5. Fluorescence spectra of α -glucosidase: (A) in the absence of compound **11j** at 20–60 °C, (B) in the presence of compound **11j** at inhibitory concentration (12.4 μ M) at 20–60 °C.

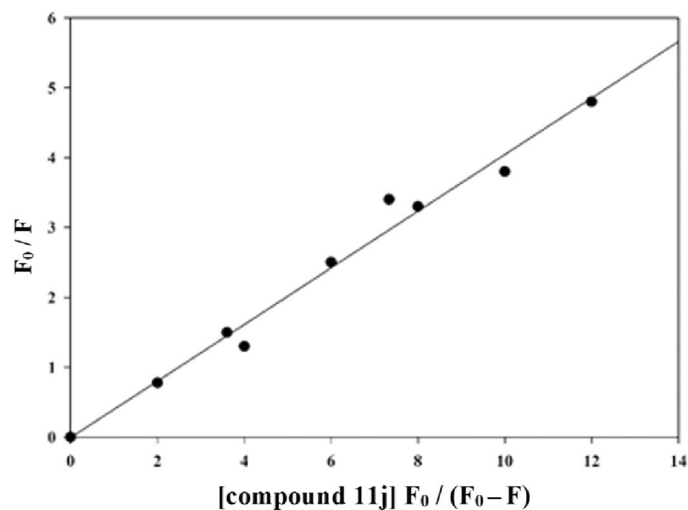


Figure 6. The plots F_0/F Vs. function of $[D_t] F_0/(F_0-F)$ at 20 °C for imidazoquinazoline **11j**.

K_A (L mol ⁻¹ s ⁻¹) ^a	K_A (L mol ⁻¹ s ⁻¹) ^b	n^b	r^b
36.6×10^4	40.5×10^4	0.3	0.997

Table 4. Binding constants and binding sites for imidazoquinazoline **11j**. ^aTemperature is 60 °C. ^bTemperature is 20 °C.

profile including ΔG (free energy change), ΔH (enthalpy change), and ΔS (entropy change) could be computed to determine the type of non-covalent forces between imidazo[1,2-*c*]quinazoline **11j** and binding site of α -glucosidase. These forces between the protein and inhibitor can be categorized into four groups: hydrogen bond, van der Waals forces, electrostatic attraction, and hydrophobic interactions. To identify the type of interactions in present study, thermodynamic parameters must be calculated using following equations:

$$\ln \frac{K_{A2}}{K_{A1}} = \frac{\Delta H}{R} \left(\frac{1}{T_2} - \frac{1}{T_1} \right) \quad (4)$$

$$\Delta G = -RT \ln K_A = \Delta H - T\Delta S \quad (5)$$

Already, there was some information including binding constants ($K_{A2} = 36.6 \times 10^4$ and $K_{A1} = 40.5 \times 10^4$) as well as initial and final temperatures ($T_1 = 20$ °C (293 K) and $T_2 = 60$ °C (333 K)). Therefore, using Eq. (4), ΔH is obtained -2.17 (kJ mol⁻¹) and subsequently using Eq. (5), ΔG and ΔS values are calculated -20.6 (kJ mol⁻¹) and 62.9 (J mol⁻¹ K⁻¹), respectively.

Considering the sign of these thermodynamic parameters, the type of non-covalent force could be determined as follow: (1) $\Delta H > 0$, $\Delta S > 0$, hydrophobic interactions; (2) $\Delta H < 0$, $\Delta S > 0$, van der Waals forces; (3) $\Delta H < 0$, $\Delta S < 0$, hydrogen bond and van der Waals interactions; and (4) $\Delta H < 0$, $\Delta S > 0$, electrostatic interactions. Therefore, the obtained results indicated that the acting force between imidazoquinazoline **11j** and α -glucosidase was mainly determined as electrostatic forces^{51,52}.

Molecular docking studies. Molecular docking study was conducted using AutoDock4 and Auto Dock Tools (version 1.5.6) to explore the interaction patterns of substituted benzo[4,5]imidazo[1,2-*c*]quinazoline **6a–c** and imidazo[1,2-*c*]quinazolines **11a–o** within the active site of human acid- α -glucosidase (PDB ID: 5NN8). This PDB ID was also used in previous studies⁵³. Observed interactions are listed in Table 5. The binding energy of imidazo[1,2-*c*]quinazolines **11a–o** were found to be in range of -7.62 to -8.59 kcal mol⁻¹, which is noticeably better than that of acarbose (-3.79 kcal mol⁻¹). The docking protocol validation involved a redocking study using the crystallized ligand with PDB ID of 5NN8. This process resulted to a low RMSD value of 1.57, confirming the reliability of our docking studies.

Additionally, the similar computational process was conducted for benzo[4,5]imidazo[1,2-*c*]quinazolines **6a–c**, showing the binding energy scores between -7.30 to -7.58 kcal mol⁻¹. These values were moderately lower than the binding energies in second series. These figures were found to be -8.07 , -7.79 , and -8.05 kcal mol⁻¹ for compounds **11a**, **11b**, and **11g**, respectively; however, they were -7.30 , -7.58 , and -7.32 kcal mol⁻¹ for compounds **6a**, **6b**, and **6c**, respectively. It might be related to its fewer interactions. This issue is illustrated by comparing compounds **6a** with **11a** as shown in Fig. 7. It must be noted no hydrogen bond formation was observed, and hydrophobic interactions are shown by dashed lines.

Compound	Binding energy (Kcal mol ⁻¹)	Interactions ^a	Moiety	Residue
11a	- 8.07	Hydrophobic interactions		
11b	- 7.79	Hydrogen bond	Imidazoquinazoline	ARG600
		π -Cation Interaction	Phenyl	ARG600
11c	- 8.02	Hydrophobic interactions		
11d	- 8.01	Hydrophobic interactions		
11e	- 7.71	Hydrogen bond	Imidazoquinazoline	ARG600
		π -Cation Interaction	Phenyl	ARG600
11f	- 8.50	π -Stacking	Phenyl	PHE649
11g	- 8.05	Hydrogen bond	methoxy	ALA284
11h	- 7.62	Hydrogen bond	Methoxy	ALA284
11i	- 7.71	Hydrophobic interactions		
11j	- 8.50	Hydrogen bond	Methoxy	ALA284
11k	- 8.35	Hydrogen bond	Methoxy	ALA284
		π -Stacking	Phenyl	PHE649
11l	- 8.28	Hydrogen bond	Methoxy	ALA284
11m	- 7.65	Hydrogen bond	Imidazoquinazoline	ARG600
		π -Cation Interaction	Phenyl	ARG600
11n	- 8.07	Hydrogen bond	Methoxy	ALA284
11o	- 8.59	Hydrogen bond	Methoxy	ALA284

Table 5. Interactions of compounds **11a–o** with crystal structure of human acid- α -glucosidase using BIOVIA Discovery Studio visualizer v21.1.0.20298 and PLIP online service. ^aHydrophobic interactions for compounds with hydrogen bonds or other types of interactions were not mentioned.

As previously described in SAR analysis, derivatives bearing electron-donating groups, particularly OMe (compounds **11e–o**), exhibited the excellent to great inhibitory activities. Herein, molecular docking studies (as presented in Table 6) revealed that these compounds **11e–o**, except **11i**, created a hydrogen bond with OMe moiety or imidazoquinazoline backbone, which might be responsible for their significant inhibitory potencies.

Imidazo[1,2-*c*]quinazoline **11j**, the most potent compound in present study with the best IC₅₀ value (12.44 ± 0.38 μ M), exhibited a noticeable binding energy of - 8.50 kcal mol⁻¹. This affinity could be attributed to the formation of a hydrogen bond between the OMe moiety at C-3 position and ALA-284 residue within the receptor. This similar hydrogen bond was observed in the complex of acarbose and receptor in the crystal structure. Additionally, compound **11j** formed several hydrophobic interactions with different residues including TRP-481, TRP-376, LEU-678, PHE-649, and ILE-441 within the active site of α -glucosidase (Fig. 8). Similar hydrophobic interactions between acarbose and some residues in the binding site of the receptor (like TRP-481 and TRP-376) were observed in the redocking results. The presence of these interactions with tryptophan residues is consistent with the results of fluorescence spectroscopy measurements. Overall, similar interactions between both compound **11j** and acarbose with active site of α -glucosidase, as well as their superimposition as depicted in Fig. 9, can confirm the accuracy of the docking procedure and the validity of results.

In silico ADME. The ADME parameters of benzo[4,5]imidazo[1,2-*c*]quinazolines **6a–c** and imidazo[1,2-*c*]quinazolines **11a–o** were calculated using SwissADME online server⁵⁴. The results are summarized in Table 6. All compounds possessed favorable drug-likeness, and they were mostly consistent with Lipinski's Rule of 5. FDA-approved α -glucosidase inhibitors, particularly acarbose, possess low oral bioavailability and act as a competitive, reversible inhibitor of membrane-bound intestinal enzyme. Considering the presence of α -glucosidase in the lumen and its mechanism, it was assumed that low Human intestinal absorption (HIA) of imidazoquinazolines **11a–o** would be a promising factor to observe minimum systemic adverse effects, while being sufficiently effective in the lumen environment^{55,56}. However, second series, including compounds **6a–c** were predicted to have high HIA, indicating their potentially lower pharmacological activities.

Since acarbose acts in the gastrointestinal tract, its low systemic absorption (below 2% of the administered dose) is crucial for optimal therapeutic efficacy⁵⁷. In Fig. 10, passive gastro-intestinal absorption (HIA) and blood-brain barrier (BBB) permeation were predicted by the BOILED-Egg model⁵⁸. In this figure, benzo[4,5]imidazo[1,2-*c*]quinazolines **6a–c** were shown by blue dots. Imidazo[1,2-*c*]quinazolines **11a–o** were shown by red dots, and some of them were overlapped by each other. Compounds which are located in the yellow region are predicted to have BBB permeability. Benzo[4,5]imidazo[1,2-*c*]quinazolines **6a–c** were predicted to be BBB permeable, which is a negative feature for using these compounds as α -glucosidase inhibitors. However, none of imidazo[1,2-*c*]quinazolines **11a–o** were anticipated to be BBB-permeable, which is ideal for α -glucosidase inhibitor safety profile.

Moreover, compounds which are located in the white area are predicted to have good absorption. As previously discussed, considering the enzyme's site of action (lumen environment), high bioavailability may cause side effects without any improvement on the efficacy. Overall, benzo[4,5]imidazo[1,2-*c*]quinazolines **6a–c** possessed

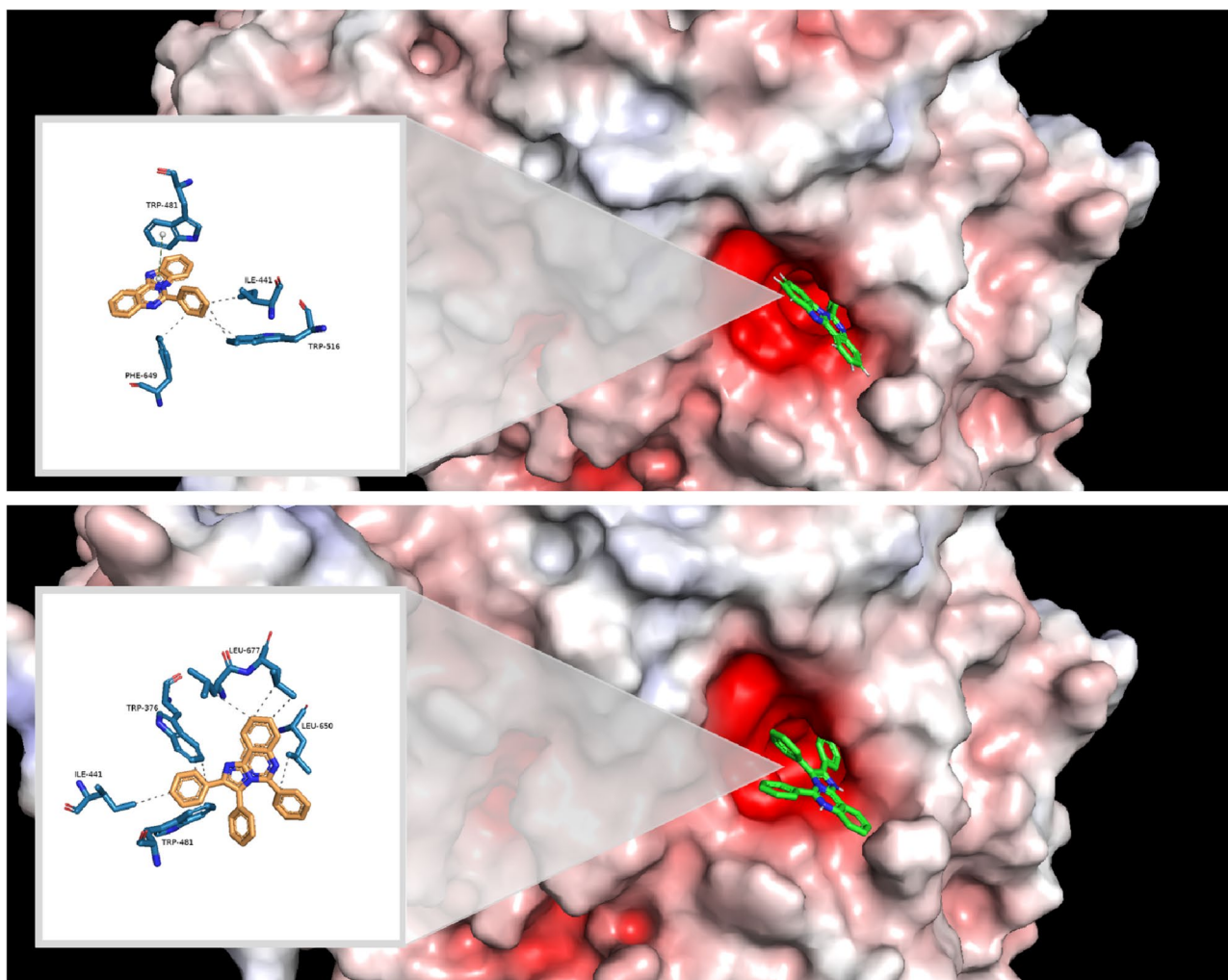


Figure 7. Interactions and structures of (a) compound **6a** and (b) compound **11a** in the binding pocket of human acid- α -glucosidase visualized using PyMOL 2.5.2 and PLIP online service.

higher bioavailability, which is not favorable for α -glucosidase inhibitory activity in the gastrointestinal tract, while imidazo[1,2-*c*]quinazolines **11a–o** were able to act locally in the lumen without getting into the bloodstream. Therefore, compounds **11a–o** with low HIA and no BBB-permeation could be potential candidates for further studies.

Conclusion

In attempt to find novel and potent α -glucosidase inhibitors, efficient synthetic approaches were performed to synthesize substituted imidazo[1,2-*c*]quinazolines **6** and **11**. Their inhibitory potencies were evaluated, showing excellent to great potencies (ranged from $12.44 \pm 0.38 \mu\text{M}$ to $308.33 \pm 0.06 \mu\text{M}$) in comparison with acarbose ($\text{IC}_{50} = 750.0 \pm 1.5 \mu\text{M}$). Notably, compound **11j** exhibited the most potent inhibitory activity, therefore, it was selected for further evaluations including kinetic analysis, circular dichroism, fluorescence spectroscopy, and thermodynamic profile. It was observed that imidazoquinazoline **11j** compete with the substrate for binding to the binding site of α -glucosidase. Moreover, circular dichroism and fluorescence spectroscopy measurements confirmed that this binding led to change the secondary and tertiary structure of enzyme and inhibit its performance. Calculation of thermodynamic parameters including ΔG (free energy change), ΔH (enthalpy change), and ΔS (entropy change) values revealed the construction of spontaneous, electrostatic forces between imidazoquinazoline **11j** and α -glucosidase. The importance of the presence of electron-donating groups such as OMe was verified during the docking procedure, since an important hydrogen bond was formed in the mentioned compounds. Also, the superiority of compounds **11** over **6** was confirmed by the low HIA figures of imidazoquinazoline **11** in ADME studies. Overall, these results showed that our target imidazoquinazolines could be considered as a promising hit for further development of α -glucosidase inhibitors as a well-established diabetes treatment approach.

Compound	MW	Consensus Log P	GI absorption	Bioavailability Score	Rotatable bonds	H-bond acceptors	H-bond donors
11a	397.47	3.78	Low	0.55	3	2	–
11b	431.92	4.06	Low	0.55	3	2	–
11c	431.92	3.92	Low	0.55	3	2	–
11d	431.92	3.93	Low	0.55	3	2	–
11e	411.50	3.96	Low	0.55	3	2	–
11f	440.54	4.08	Low	0.55	4	3	–
11g	427.50	3.91	Low	0.55	4	3	–
11h	427.50	4.2	Low	0.55	5	4	–
11i	427.50	3.9	Low	0.55	4	2	–
11j	457.52	4.15	Low	0.55	5	4	–
11k	457.52	4.11	Low	0.55	5	4	–
11l	457.52	4.09	Low	0.55	6	5	–
11m	457.52	4.22	Low	0.55	5	4	–
11n	487.55	4.02	Low	0.55	4	3	–
11o	536.42	4.05	Low	0.17	5	4	–
6a	295.34	4.11	High	0.55	2	0	–
6b	329.78	4.69	High	0.55	2	0	–
6c	325.36	4.15	High	0.55	3	0	–

Table 6. The prediction of pharmacokinetic's parameters of imidazoquinazolines 11a–o and 6a–c by SWISSADME.

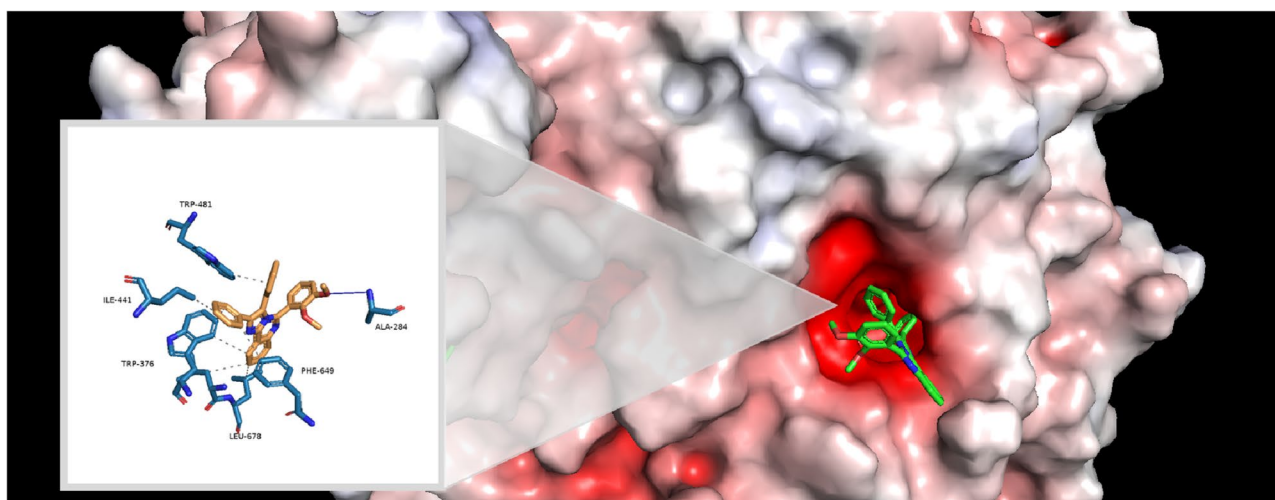


Figure 8. The interactions and structure of compound 11j in the binding pocket of human acid- α -glucosidase (it must be noted that the hydrogen bond and hydrophobic interactions are displayed in blue color and dashed lines, respectively).

Experimental

All chemicals were purchased from Merck (Germany) and were used without further purification. Melting points were measured on an Electrothermal 9100 apparatus. Elemental analyses for C, H and N were performed using a Heraeus CHN-O-Rapid analyzer. Mass spectra were recorded on an Agilent Technologies (HP) 5973 mass spectrometer operating at an ionization potential of 20 eV. IR spectra were recorded on a Shimadzu IR-460 spectrometer. ^1H and ^{13}C NMR spectra were measured (DMSO- d_6 solution) with Bruker DRX-300 (at 300.1 and 75.5 MHz) and Bruker DRX-500 AVANCE (at 500.1 and 125.8 MHz) instruments.

General synthetic procedures. *General procedure for the preparation of 2-(2-Nitrophenyl)-1H-benzo[d]imidazole 3:* A mixture of 2-nitrobenzaldehyde **1** (8.0 mmol, 1.208 g), benzene-1,2-diamine **2** (6.7 mmol, 0.723 g), and glacial acetic acid (20 mol%, 1.34 mmol, 0.076 ml) in EtOH (15 ml) was heated reflux conditions within 10 h. As the completion of compound **3** was confirmed by TLC analysis, the reaction mixture was quenched by water, and the resulting precipitation was filtered and washed completely. Afterwards, it was

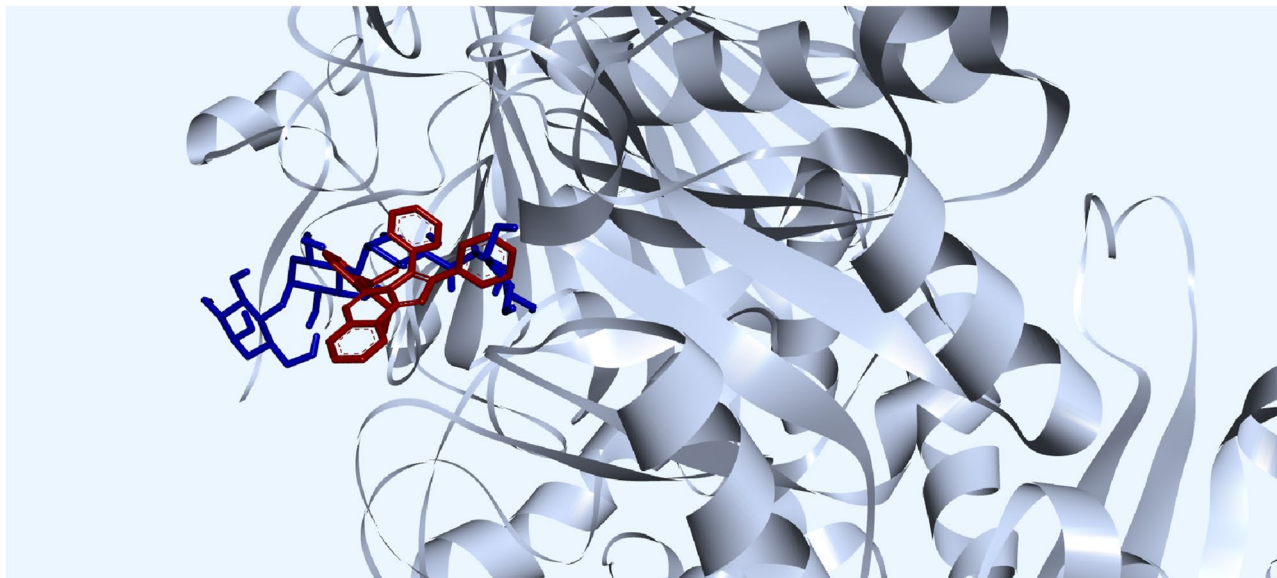


Figure 9. Superimposition of acarbose and compound **11j** in the binding pocket of human acid- α -glucosidase. Acarbose is colored in blue, and compound **11j** is colored in red.

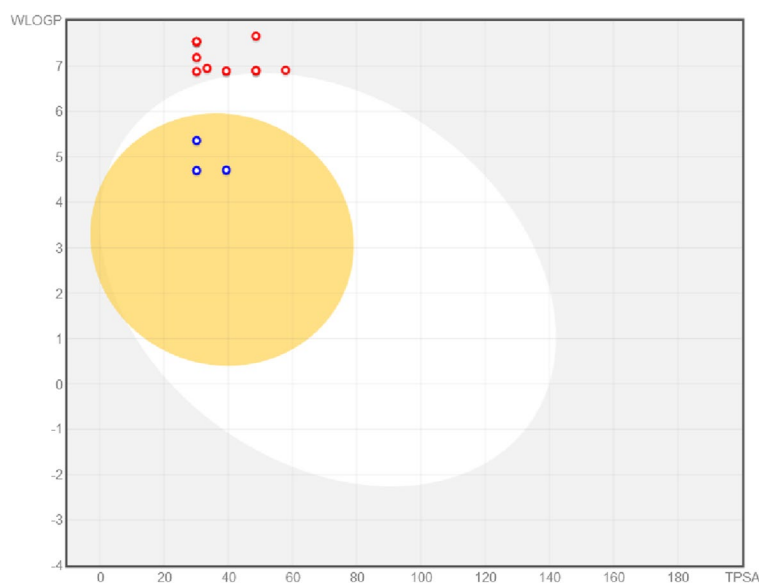


Figure 10. Compounds **6a–c** and **11a–o** were examined by the boiled-egg method available on SWISS ADME.

recrystallized by EtOAc and *n*-Hexane (within the proportion of 3:1) to afford the desirable compound **3** as a pure orange solid in 78% yield.

2-(2-Nitrophenyl)-1H-benzo[d]imidazole 3: Orange solid, mp 264–267 °C, yield: 78%. IR (KBr) ($\nu_{\max}/\text{cm}^{-1}$): 3329 (NH), 1622, 1553, 1488, 1403, 1396, 1348, 1285, 1233, 1177, 1093, 1061, 949, 913, 880, 858, 746, 693. ^1H NMR (500.1 MHz, DMSO- d_6): δ 10.78 (br s., 1H, NH), 8.03 (d, $J=8.2$ Hz, 1H, CH), 7.99 (d, $J=7.7$ Hz, 1H, CH), 7.86 (t, $J=7.6$ Hz, 1H, CH), 7.74 (t, $J=7.3$ Hz, 1H, CH), 7.71–7.60 (m, 2H, 2CH), 7.30–7.20 (m, 2H, 2CH). ^{13}C NMR (125.8 MHz, DMSO- d_6): δ 150.55, 147.43, 143.38, 135.49, 133.24, 131.92, 130.98, 124.78, 123.12, 120.13, 112.78. ESI-MS m/z : 240.48 [$M+1$] $^+$. Anal. Calcd. for $\text{C}_{13}\text{H}_9\text{N}_3\text{O}_2$: C, 65.27; H, 3.79; N, 17.56; found: C, 65.08; H, 4.05; N, 17.78%.

General procedure for the preparation of 2-(2-Nitrophenyl)-4,5-diphenyl-1H-imidazole 9. A mixture of 2-nitrobenzaldehyde **1** (36 mmol, 5.436 g), benzil **7** (30 mmol, 6.302 g), and ammonium acetate **8** (300 mmol, 23.125 g) in glacial acetic acid (75 ml) were heated under the reflux conditions for 10 h. After completion of the reaction, which was monitored by TLC, the mixture was cooled down to room temperature, and it was gradually poured into crushed ice. The yellow solid residue got to precipitate, filtered, and washed with water. Finally, it was recrystallized from EtOH (40 ml) to obtain the pure adduct **9** as yellow powder in 84% yield.

2-(2-Nitrophenyl)-4,5-diphenyl-1H-imidazole **9**: Yellow solid, mp 236–240 °C, yield: 84%. IR (KBr) ($\nu_{\max}/\text{cm}^{-1}$): 3348 (NH), 1592, 1549, 1487, 1436, 1396, 1343, 1296, 1247, 1168, 1108, 1089, 974, 903, 849, 826, 737, 640. ^1H NMR (500.1 MHz, DMSO- d_6): δ 10.23 (br s., 1H, NH), 8.29 (d, $J=8.0$ Hz, 1H, CH), 7.98 (d, $J=7.8$ Hz, 1H, CH), 7.70 (t, $J=7.7$ Hz, 1H, CH), 7.62 (t, $J=7.5$ Hz, 1H, CH), 7.38–7.20 (m, 10H, 10CH). ^{13}C NMR (125.8 MHz, DMSO- d_6): δ 148.98, 146.38, 141.09, 134.75, 133.30, 132.21, 130.68, 128.45, 127.74, 125.91, 124.68. ESI–MS m/z : 342.84 $[\text{M}+1]^+$. Anal. Calcd. for $\text{C}_{21}\text{H}_{15}\text{N}_3\text{O}_2$: C, 73.89; H, 4.43; N, 12.31.; found: C, 74.12; H, 4.68; N, 12.56%.

General procedure for the reduction of nitro functionality to amine moiety (compounds 4 and 10). The procedure was common for both series: to a mixture of 2-(2-Nitrophenyl)-1H-benzo[d]imidazole **4** (5.20 mmol, 1.243 g) in hydrochloric acid (12.48 ml) and MeOH (5 ml) in ice bath at 0 °C, stannous chloride dihydrate $\text{SnCl}_2 \cdot 2\text{H}_2\text{O}$ (17.16 mmol, 3.878 g) was added gradually within 1 h. Afterwards, the mixture was stirred at room temperature for almost 6 h till the yellow color of nitro moiety got disappeared. As compound **3** was completely used, and it was confirmed by TLC analysis, the reaction mixture was basified by a solution of NaOH (2N) to pH 8. Then, water (20 ml) was added to the mixture and extracted three times with EtOAc (3 \times 45 ml). The combined organic extracts were washed with brine, dried over Na_2SO_4 , and then concentrated. The precipitate was filtered and washed with Et_2O to afford pure product **4** as white powder in 58% yield.

2-(1H-benzo[d]imidazol-2-yl)aniline **4**: White solid, mp 208–211 °C, yield: 58%. IR (KBr) ($\nu_{\max}/\text{cm}^{-1}$): 3184, 3058, and 3024 (3NH), 1611, 1519, 1476, 1429, 1279, 1178, 1056, 908, 882, 795, 723, 689, 633. ^1H NMR (500.1 MHz, DMSO- d_6): δ 7.81 (d, $J=7.8$ Hz, 1H, CH), 7.76–7.69 (m, 2H, 2CH), 7.62–7.54 (m, 2H, 2CH), 7.49 (t, $J=7.8$ Hz, 1H, CH), 7.10 (t, $J=7.5$ Hz, 1H, CH), 6.68 (dd, $J=7.3$ and 0.9 Hz, 1H, CH), 3.84–3.42 (br s, 3H, NH and NH_2). ^{13}C NMR (125.8 MHz, DMSO- d_6): δ 153.78, 147.86, 138.56, 131.08, 127.98, 122.76, 117.66, 115.38, 114.93, 110.38. ESI–MS m/z : 209.96 $[\text{M}]^+$. Anal. Calcd. for $\text{C}_{13}\text{H}_{11}\text{N}_3$: C, 74.62; H, 5.30; N, 20.08.; found: C, 74.49; H, 5.08; N, 20.23%.

In a similar procedure, 2-(2-Nitrophenyl)-4,5-diphenyl-1H-imidazole **4** (25.2 mmol, 8.593 g) in hydrochloric acid (60.48 ml) and MeOH (30 ml) in ice bath at 0 °C, stannous chloride dihydrate $\text{SnCl}_2 \cdot 2\text{H}_2\text{O}$ (83.16 mmol, 18.794 g) was added slowly within 1 h. The reaction took 4 h to get finish. After workup, pure white powder compound **10** was obtained in 63% yield.

2-(4,5-diphenyl-1H-imidazol-2-yl)aniline **10**: White solid, mp 218–220 °C, yield: 63%. IR (KBr) ($\nu_{\max}/\text{cm}^{-1}$): 3408, 3369, and 3238 (3NH), 1622, 1467, 1417, 1297, 1233, 1177, 1093, 1061, 949, 913, 869, 844, 758, 673. ^1H NMR (500.1 MHz, DMSO- d_6): δ 10.24 (s, 1H, NH), 7.96 (d, $J=7.8$ Hz, 1H, CH), 7.53–7.20 (m, 11H, 11CH), 6.94 (t, $J=7.6$ Hz, 1H, CH), 6.68 (d, $J=7.4$ Hz, 1H, CH), 5.23 (s, 2H, NH_2). ^{13}C NMR (125.8 MHz, DMSO- d_6): δ 147.36, 146.98, 135.87, 132.45, 129.65, 128.78, 127.65, 126.24, 116.84, 115.53, 111.64. ESI–MS m/z : 311.78 $[\text{M}]^+$. Anal. Calcd. for $\text{C}_{21}\text{H}_{17}\text{N}_3$: C, 81.00; H, 5.50; N, 13.49.; found: C, 80.82; H, 5.39; N, 13.75%.

General procedure for the preparation of poly-substituted imidazo[1,2-c]quinazolines 6a-c and 11a-o. A mixture of synthesized 2-(1H-benzo[d]imidazol-2-yl)aniline **4** or 2-(4,5-diphenyl-1H-imidazol-2-yl)aniline **10** (1 mmol, g) with corresponding substituted benzaldehyde **5** (1.5 mmol) in glacial acetic acid (5 ml) was magnetically stirred at 80 °C for almost 3 to 4 h. After completion of reaction confirmed by TLC analysis, the mixture was cooled to the room temperature and poured into water. The precipitate was filtered, washed with water, and recrystallized from EtOAc to obtain the desired imidazoquinazolines **6a–c** and **11a–o** as pure powder in good to excellent yields.

6-phenylbenzo[4,5]imidazo[1,2-c]quinazoline **6a**: Yellow solid, mp 156–158 °C, yield: 86%. IR (KBr) ($\nu_{\max}/\text{cm}^{-1}$): 1596, 1498, 1433, 1378, 1294, 1263, 1182, 1123, 1082, 993, 825, 755, 685, 634. ^1H NMR (500.1 MHz, DMSO- d_6): δ 8.23 (d, $J=7.8$ Hz, 1H, CH), 8.16 (d, $J=7.7$ Hz, 1H, CH), 7.74 (d, $J=8.0$ Hz, 1H, CH), 7.40–7.16 (m, 8H, 8CH), 6.95 (d, $J=7.9$ Hz, 1H, CH), 6.86 (t, $J=7.4$ Hz, 1H, CH). ^{13}C NMR (125.8 MHz, DMSO- d_6): δ 145.47, 144.13, 139.07, 136.66, 134.20, 130.87, 129.48, 129.05, 128.98, 126.20, 125.79, 124.57, 124.11, 118.43, 115.87, 115.22, 111.83, 107.42. ESI–MS m/z : 295.87 $[\text{M}]^+$. Anal. Calcd. for $\text{C}_{20}\text{H}_{13}\text{N}_3$: C, 81.34; H, 4.44; N, 14.23.; found: C, 81.66; H, 4.28; N, 13.99%.

6-(4-chlorophenyl)benzo[4,5]imidazo[1,2-c]quinazoline **6b**: Yellow solid, mp 173–175 °C, yield: 92%. IR (KBr) ($\nu_{\max}/\text{cm}^{-1}$): 1526, 1487, 1423, 1385, 1348, 1343, 1288, 1225, 1173, 1074, 1042, 1013, 911, 845, 827, 780, 769, 697. ^1H NMR (500.1 MHz, DMSO- d_6): δ 7.94 (d, $J=7.6$ Hz, 1H, CH), 7.63 (d, $J=7.9$ Hz, 1H, CH), 7.52 (d, $J=7.4$ Hz, 1H, CH), 7.30–6.92 (m, 7H, 7CH), 6.84 (d, $J=7.8$ Hz, 1H, CH), 6.81 (t, $J=7.2$ Hz, 1H, CH). ^{13}C NMR (125.8 MHz, DMSO- d_6): δ 146.91, 143.55, 143.24, 138.42, 137.44, 132.77, 129.59, 129.26, 127.41, 126.28, 124.66, 122.24, 122.08, 118.52, 118.15, 114.81, 111.70, 110.60. ESI–MS m/z : 329.43 $[\text{M}]^+$. Anal. Calcd. for $\text{C}_{20}\text{H}_{12}\text{ClN}_3$: C, 72.84; H, 3.67; N, 12.74.; found: C, 73.06; H, 3.42; N, 12.96%.

6-(4-methoxyphenyl)benzo[4,5]imidazo[1,2-c]quinazoline **6c**: Yellow solid, mp 198–201 °C, yield: 79%. IR (KBr) ($\nu_{\max}/\text{cm}^{-1}$): 1592, 1498, 1403, 1387, 1292, 1226, 1198, 1132, 1068, 1015, 937, 847, 785, 769, 684, 623. ^1H NMR (500.1 MHz, DMSO- d_6): δ 7.95 (d, $J=7.6$ Hz, 1H, CH), 7.63 (d, $J=7.9$ Hz, 1H, CH), 7.48 (d, $J=7.8$ Hz, 1H, CH), 7.32–6.90 (m, 6H, 6CH), 6.88 (d, $J=8.2$ Hz, 2H, 2CH), 6.81 (t, $J=7.8$ Hz, 1H, CH), 3.68 (s, 3H, OCH_3). ^{13}C NMR (125.8 MHz, DMSO- d_6): δ 159.72, 146.97, 143.62, 143.39, 132.80, 132.34, 131.69, 130.42, 127.52, 124.67, 122.18, 122.03, 118.52, 118.14, 114.80, 114.09, 111.72, 110.66, 55.15. ESI–MS m/z : 310.74 $[\text{M}+1]^+$. Anal. Calcd. for $\text{C}_{21}\text{H}_{15}\text{N}_3\text{O}$: C, 84.53; H, 4.89; N, 13.58.; found: C, 84.76; H, 5.14; N, 13.84%.

2,3,5-triphenylimidazo[1,2-c]quinazoline **11a**: Milky solid, mp 133–137 °C, yield: 78%. IR (KBr) ($\nu_{\max}/\text{cm}^{-1}$): 1598, 1496, 1456, 1412, 1368, 1289, 1263, 1148, 1129, 1067, 1026, 989, 965, 897, 822, 752, 689, 636. ^1H NMR (500.1 MHz, DMSO- d_6): δ 7.88 (d, $J=7.5$ Hz, 1H, CH), 7.50 (d, $J=7.2$ Hz, 2H, 2CH), 7.45–7.00 (m, 14H, 14CH), 6.84 (d, $J=7.1$ Hz, 1H, CH), 6.82 (t, $J=6.9$ Hz, 1H, CH). ^{13}C NMR (125.8 MHz, DMSO- d_6): δ 141.37, 140.93, 137.50, 133.94, 130.32, 130.13, 129.38, 129.05, 128.91, 128.54, 128.37, 128.18, 126.42, 125.10, 124.86, 123.19,

122.82, 113.24. ESI-MS m/z : 397.26 $[M]^+$. Anal. Calcd. for $C_{28}H_{19}N_3$: C, 84.61; H, 4.82; N, 10.57; found: C, 84.93; H, 4.62; N, 10.78%.

5-(4-chlorophenyl)-2,3-diphenylimidazo[1,2-*c*]quinazoline **11b**: Milky solid, mp 178–181 °C, yield: 94%. IR (KBr) ($\nu_{\max}/\text{cm}^{-1}$): 1589, 1488, 1463, 1399, 1348, 1294, 1231, 1168, 1129, 1087, 996, 929, 886, 795, 756, 718, 675, 638. ^1H NMR (500.1 MHz, DMSO- d_6): δ 7.90 (d, $J=7.2$ Hz, 1H, CH), 7.50 (d, $J=7.8$ Hz, 2H, 2CH), 7.42–7.00 (m, 13H, 13CH), 6.96 (d, $J=7.9$ Hz, 1H, CH), 6.85 (t, $J=7.6$ Hz, 1H, CH). ^{13}C NMR (125.8 MHz, DMSO- d_6): δ 141.13, 140.80, 139.66, 137.17, 133.42, 133.02, 130.35, 129.10, 129.02, 128.57, 128.20, 127.10, 126.84, 126.60, 126.38, 123.33, 122.97, 112.73. ESI-MS m/z : 431.86 $[M]^+$. Anal. Calcd. for $C_{28}H_{18}ClN_3$: C, 77.86; H, 4.20; N, 9.73; found: C, 78.04; H, 4.06; N, 9.53%.

5-(3-chlorophenyl)-2,3-diphenylimidazo[1,2-*c*]quinazoline **11c**: Milky solid, mp 149–151 °C, yield: 83%. IR (KBr) ($\nu_{\max}/\text{cm}^{-1}$): 1586, 1509, 1447, 1367, 1320, 1286, 1184, 1129, 1068, 1023, 967, 834, 754, 685, 622. ^1H NMR (300.1 MHz, DMSO- d_6): δ 7.97 (d, $J=7.7$ Hz, 1H, CH), 7.76 (d, $J=7.9$ Hz, 2H, 2CH), 7.60–7.17 (m, 11H, 11CH), 7.11 (d, $J=8.0$ Hz, 2H, 2CH), 6.91 (d, $J=7.2$ Hz, 1H, CH), 6.79 (t, $J=7.6$ Hz, 1H, CH). ^{13}C NMR (75.1 MHz, DMSO- d_6): δ 141.81, 141.10, 135.39, 131.27, 131.06, 130.80, 129.62, 129.55, 129.50, 129.10, 128.99, 128.76, 128.69, 127.15, 127.02, 126.95, 125.42, 123.67, 119.06, 115.63. ESI-MS m/z : 432.29 $[M+1]^+$. Anal. Calcd. for $C_{28}H_{18}ClN_3$: C, 77.86; H, 4.20; N, 9.73; found: C, 77.94; H, 4.13; N, 9.89%.

5-(2-chlorophenyl)-2,3-diphenylimidazo[1,2-*c*]quinazoline **11d**: Milky solid, mp 164–167 °C, yield: 72%. IR (KBr) ($\nu_{\max}/\text{cm}^{-1}$): 1599, 1498, 1438, 1399, 1358, 1294, 1256, 1162, 1129, 1089, 1012, 991, 932, 899, 836, 763, 729, 687, 624. ^1H NMR (500.1 MHz, DMSO- d_6): δ 8.04 (d, $J=8.0$ Hz, 1H, CH), 7.87 (dd, $J=7.2$, 0.9 Hz, 1H, CH), 7.74 (t, $J=7.7$ Hz, 2H, 2CH), 7.68–7.17 (m, 13H, 13CH), 6.96 (d, $J=7.4$ Hz, 1H, CH), 6.83 (t, $J=7.8$ Hz, 1H, CH). ^{13}C NMR (125.8 MHz, DMSO- d_6): δ 147.90, 144.90, 138.14, 137.79, 136.29, 135.96, 133.42, 131.58, 130.82, 130.11, 129.81, 129.10, 128.30, 127.74, 127.25, 126.35, 124.84, 123.57, 119.94, 113.92. ESI-MS m/z : 432.56 $[M]^+$. Anal. Calcd. for $C_{28}H_{18}ClN_3$: C, 77.86; H, 4.20; N, 9.73; found: C, 78.06; H, 4.54; N, 9.48%.

5-(4-methylphenyl)-2,3-diphenylimidazo[1,2-*c*]quinazoline **11e**: Milky solid, mp 155–157 °C, yield: 87%. IR (KBr) ($\nu_{\max}/\text{cm}^{-1}$): 1595, 1489, 1402, 1387, 1285, 1216, 1194, 1143, 1098, 1034, 995, 865, 746, 658, 624. ^1H NMR (500.1 MHz, DMSO- d_6): δ 7.96 (d, $J=7.8$ Hz, 1H, CH), 7.84 (d, $J=7.8$ Hz, 1H, CH), 7.78 (s, 1H, CH), 7.70–7.00 (m, 13H, 13CH), 6.96 (d, $J=7.8$ Hz, 1H, CH), 6.82 (t, $J=7.4$ Hz, 1H, CH), 2.15 (s, 3H, CH₃). ^{13}C NMR (125.8 MHz, DMSO- d_6): δ 141.42, 141.04, 138.06, 137.64, 137.52, 134.05, 130.27, 130.02, 129.45, 129.05, 128.15, 126.55, 126.35, 125.04, 124.74, 123.13, 122.76, 113.47, 20.57. ESI-MS m/z : 412.37 $[M+1]^+$. Anal. Calcd. for $C_{29}H_{21}N_3$: C, 84.64; H, 5.14; N, 10.21; found: C, 84.78; H, 4.98; N, 10.38%.

4-(2,3-diphenylimidazo[1,2-*c*]quinazolin-5-yl)-*N,N*-dimethylaniline **11f**: Milky solid, mp 208–210 °C, yield: 76%. IR (KBr) ($\nu_{\max}/\text{cm}^{-1}$): 1594, 1487, 1438, 1422, 1368, 1276, 1239, 1188, 1052, 1028, 985, 913, 852, 758, 695. ^1H NMR (500.1 MHz, DMSO- d_6): δ 8.12 (d, $J=8.1$ Hz, 2H, 2CH), 7.91 (d, $J=7.8$ Hz, 1H, CH), 7.53 (d, $J=7.5$ Hz, 2H, 2CH), 7.48–7.00 (m, 9H, 9CH), 6.92 (d, $J=7.7$ Hz, 1H, CH), 6.80 (t, $J=7.4$ Hz, 1H, CH), 6.53 (d, $J=8.1$ Hz, 2H, 2CH), 2.81 (s, 6H, 2 NCH₃). ^{13}C NMR (125.8 MHz, DMSO- d_6): δ 154.65, 141.92, 141.32, 134.15, 130.07, 129.18, 129.09, 128.97, 128.60, 128.26, 127.20, 126.81, 126.74, 126.35, 124.96, 123.07, 112.28, 111.52, 31.44. ESI-MS m/z : 441.69 $[M+1]^+$. Anal. Calcd. for $C_{30}H_{24}N_4$: C, 81.79; H, 5.49; N, 12.72; found: C, 82.02; H, 5.72; N, 12.48%.

5-(4-methoxyphenyl)-2,3-diphenylimidazo[1,2-*c*]quinazoline **11g**: Milky solid, mp 189–192 °C, yield: 79%. IR (KBr) ($\nu_{\max}/\text{cm}^{-1}$): 1599, 1496, 1428, 1392, 1348, 1294, 1223, 1188, 1138, 1094, 1046, 991, 952, 889, 836, 756, 733, 678, 633. ^1H NMR (500.1 MHz, DMSO- d_6): δ 7.97 (d, $J=7.4$ Hz, 1H, CH), 7.70–7.06 (m, 13H, 13CH), 6.94 (d, $J=7.8$ Hz, 1H, CH), 6.85 (t, $J=7.5$ Hz, 1H, CH), 6.76 (d, $J=7.8$ Hz, 2H, 2CH), 3.65 (s, 3H, OCH₃). ^{13}C NMR (125.8 MHz, DMSO- d_6): δ 158.91, 148.21, 144.89, 138.18, 136.99, 136.79, 136.41, 130.27, 129.85, 129.66, 129.22, 128.64, 127.94, 127.35, 124.86, 120.02, 113.90, 111.51, 55.11. ESI-MS m/z : 427.83 $[M]^+$. Anal. Calcd. for $C_{29}H_{21}N_3O$: C, 81.48; H, 4.95; N, 9.83; found: C, 81.34; H, 5.12; N, 10.04%.

5-(3-methoxyphenyl)-2,3-diphenylimidazo[1,2-*c*]quinazoline **11h**: Milky solid, mp 174–176 °C, yield: 87%. IR (KBr) ($\nu_{\max}/\text{cm}^{-1}$): 1595, 1498, 1422, 1377, 1287, 1253, 1163, 1109, 1096, 1034, 987, 857, 763, 749, 684, 633. ^1H NMR (300.1 MHz, DMSO- d_6): δ 7.86 (d, $J=7.4$ Hz, 1H, CH), 7.50 (d, $J=7.5$ Hz, 2H, 2CH), 7.45–7.00 (m, 10H, 10CH), 6.90–6.70 (m, 3H, 3CH), 6.41 (d, $J=7.6$ Hz, 1H, CH), 6.35 (s, 1H, CH), 3.58 (s, 3H, OCH₃). ^{13}C NMR (75.1 MHz, DMSO- d_6): δ 159.12, 142.52, 141.44, 141.07, 137.56, 134.01, 130.30, 130.10, 129.79, 129.41, 129.09, 128.90, 128.18, 126.61, 126.41, 123.15, 122.79, 113.36, 111.52, 110.86, 54.94. ESI-MS m/z : 428.44 $[M+1]^+$. Anal. Calcd. for $C_{29}H_{21}N_3O$: C, 81.48; H, 4.95; N, 9.83; found: C, 81.62; H, 5.23; N, 9.68%.

5-(2-methoxyphenyl)-2,3-diphenylimidazo[1,2-*c*]quinazoline **11i**: Milky solid, mp 148–152 °C, yield: 69%. IR (KBr) ($\nu_{\max}/\text{cm}^{-1}$): 1593, 1472, 1436, 1399, 1358, 1276, 1212, 1196, 1153, 1090, 1041, 1023, 975, 856, 795, 769, 713, 642, 625. ^1H NMR (300.1 MHz, DMSO- d_6): δ 7.88 (d, $J=7.1$ Hz, 1H, CH), 7.50 (d, $J=6.9$ Hz, 2H, 2CH), 7.45–6.98 (m, 10H, 10CH), 6.95–6.85 (m, 2H, 2CH), 6.78 (t, $J=7.3$ Hz, 1H, CH), 6.71 (d, $J=7.6$ Hz, 1H, CH), 6.37 (d, $J=7.3$ Hz, 1H, CH), 3.64 (s, 3H, OCH₃). ^{13}C NMR (75.1 MHz, DMSO- d_6): δ 154.87, 141.90, 141.00, 137.85, 134.34, 130.30, 130.11, 129.88, 129.58, 128.85, 128.70, 128.30, 128.12, 126.42, 126.18, 122.93, 122.58, 113.32, 111.46, 111.22, 55.54. ESI-MS m/z : 428.44 $[M+1]^+$. Anal. Calcd. for $C_{29}H_{21}N_3O$: C, 81.48; H, 4.95; N, 9.83; found: C, 81.34; H, 4.78; N, 10.04%.

5-(2,3-dimethoxyphenyl)-2,3-diphenylimidazo[1,2-*c*]quinazoline **11j**: Milky solid, mp 221–224 °C, yield: 63%. IR (KBr) ($\nu_{\max}/\text{cm}^{-1}$): 1597, 1502, 1437, 1411, 1379, 1292, 1229, 1143, 1077, 1027, 991, 943, 899, 847, 788, 753, 706, 686, 652. ^1H NMR (500.1 MHz, DMSO- d_6): δ 8.06 (d, $J=8.5$ Hz, 1H, CH), 7.51 (d, $J=7.4$ Hz, 2H, 2CH), 7.48–7.10 (m, 10H, 10CH), 6.95 (d, $J=8.2$ Hz, 1H, CH), 6.87 (d, $J=7.9$ Hz, 1H, CH), 6.82 (t, $J=8.3$ Hz, 1H, CH), 6.05 (d, $J=7.8$ Hz, 1H, CH), 3.90 and 3.75 (2s, 6H, 2OCH₃). ^{13}C NMR (125.8 MHz, DMSO- d_6): δ 152.70, 151.86, 144.72, 141.90, 141.51, 133.58, 132.15, 131.02, 129.73, 129.52, 128.78, 127.10, 126.75, 124.50, 123.90, 118.76, 117.24, 115.69, 113.90, 108.38, 60.20, 56.19. ESI-MS m/z : 457.96 $[M]^+$. Anal. Calcd. for $C_{30}H_{23}N_3O_2$: C, 78.75; H, 5.07; N, 9.18; found: C, 78.99; H, 5.23; N, 9.36%.

5-(2,4-dimethoxyphenyl)-2,3-diphenylimidazo[1,2-*c*]quinazoline **11k**: Milky solid, mp 197–200 °C, yield: 71%. IR (KBr) ($\nu_{\max}/\text{cm}^{-1}$): 1589, 1456, 1398, 1361, 1273, 1237, 1198, 1104, 1036, 1021, 998, 943, 836, 759, 724,

639. ^1H NMR (500.1 MHz, DMSO- d_6): δ 8.06 (d, J = 8.5 Hz, 1H, CH), 7.53–7.00 (m, 11H, 11CH), 6.95–6.65 (m, 4H, 4CH), 6.05 (s, 1H, CH), 3.54 and 3.51 (2s, 6H, 2OCH₃). ^{13}C NMR (125.8 MHz, DMSO- d_6): δ 153.14, 151.88, 149.77, 142.12, 141.61, 137.31, 130.84, 129.77, 129.39, 128.92, 128.60, 128.20, 127.44, 126.88, 124.11, 118.81, 115.57, 114.12, 113.12, 112.89, 56.48, 55.65. ESI–MS m/z : 457.53 [M]⁺. Anal. Calcd. for C₃₀H₂₃N₃O₂: C, 78.75; H, 5.07; N, 9.18.; found: C, 78.58; H, 4.96; N, 8.92%.

5-(2,5-dimethoxyphenyl)-2,3-diphenylimidazo[1,2-*c*]quinazoline **11i**: Milky solid, mp 183–186 °C, yield: 67%. IR (KBr) ($\nu_{\text{max}}/\text{cm}^{-1}$): 1597, 1512, 1489, 1423, 1395, 1335, 1295, 1258, 1183, 1124, 1075, 1031, 992, 968, 899, 831, 796, 740, 685, 673, 642. ^1H NMR (500.1 MHz, DMSO- d_6): δ 7.88 (d, J = 7.6 Hz, 1H, CH), 7.60–7.00 (m, 11H, 11CH), 6.05 (s, 1H, CH), 6.94 (d, J = 7.8 Hz, 1H, CH), 6.80 (t, J = 8.0 Hz, 1H, CH), 6.48 (s, 1H, CH), 6.33 (d, J = 7.5 Hz, 1H, CH), 6.29 (d, J = 7.5 Hz, 1H, CH), 3.54 and 3.51 (2s, 6H, 2OCH₃). ^{13}C NMR (125.8 MHz, DMSO- d_6): δ 161.11, 156.52, 142.30, 141.66, 138.00, 132.84, 130.63, 130.30, 129.33, 129.20, 128.62, 126.81, 126.41, 123.28, 121.32, 118.75, 117.01, 115.63, 105.05, 99.04, 56.11, 55.62. ESI–MS m/z : 458.64 [M + 1]⁺. Anal. Calcd. for C₃₀H₂₃N₃O₂: C, 78.75; H, 5.07; N, 9.18.; found: C, 78.93; H, 5.26; N, 9.33%.

5-(3,4-dimethoxyphenyl)-2,3-diphenylimidazo[1,2-*c*]quinazoline **11m**: Milky solid, mp 234–237 °C, yield: 84%. IR (KBr) ($\nu_{\text{max}}/\text{cm}^{-1}$): 1595, 1522, 1424, 1386, 1296, 1259, 1178, 1154, 1078, 1014, 997, 947, 923, 805, 768, 743, 695, 629. ^1H NMR (300.1 MHz, DMSO- d_6): δ 8.04 (d, J = 7.2 Hz, 1H, CH), 7.65–7.15 (m, 11H, 11CH), 6.91 (d, J = 6.9 Hz, 1H, CH), 6.85 (t, J = 7.5 Hz, 1H, CH), 6.77 (d, J = 8.1 Hz, 1H, CH), 6.64 (s, 2H, 2CH), 6.33 (d, J = 8.1 Hz, 1H, CH), 3.64 and 3.57 (2s, 6H, 2OCH₃). ^{13}C NMR (75.8 MHz, DMSO- d_6): δ 156.31, 155.22, 149.29, 148.94, 142.30, 141.30, 133.04, 131.80, 130.88, 129.66, 129.31, 129.01, 128.36, 128.04, 124.26, 119.09, 117.71, 115.73, 111.84, 109.70, 55.84, 55.82. ESI–MS m/z : 458.32 [M + 1]⁺. Anal. Calcd. for C₃₀H₂₃N₃O₂: C, 78.75; H, 5.07; N, 9.18.; found: C, 78.92; H, 4.87; N, 9.36%.

2,3-diphenyl-5-(3,4,5-trimethoxyphenyl)imidazo[1,2-*c*]quinazoline **11n**: Milky solid, mp 256–260 °C, yield: 78%. IR (KBr) ($\nu_{\text{max}}/\text{cm}^{-1}$): 1595, 1539, 1426, 1399, 1358, 1289, 1243, 1167, 1143, 1089, 1045, 987, 935, 829, 778, 685, 645. ^1H NMR (300.1 MHz, DMSO- d_6): δ 8.07 (d, J = 7.0 Hz, 1H, CH), 7.60–7.12 (m, 11H, 11CH), 6.97 (d, J = 8.1 Hz, 1H, CH), 6.87 (t, J = 7.4 Hz, 1H, CH), 6.23 (s, 2H, 2CH), 3.56 and 3.53 (2s, 9H, 3OCH₃). ^{13}C NMR (75.1 MHz, DMSO- d_6): δ 156.79, 155.21, 146.36, 141.69, 139.71, 138.88, 137.07, 134.82, 130.89, 130.63, 130.39, 129.78, 129.36, 128.89, 128.42, 124.83, 120.04, 115.26, 58.36, 56.72. ESI–MS m/z : 488.26 [M + 1]⁺. Anal. Calcd. for C₃₁H₂₅N₃O₃: C, 76.37; H, 5.17; N, 8.62.; found: C, 76.18; H, 4.98; N, 8.48%.

5-(3-bromo-4,5-dimethoxyphenyl)-2,3-diphenylimidazo[1,2-*c*]quinazoline **11o**: Milky solid, mp 287–289 °C, yield: 90%. IR (KBr) ($\nu_{\text{max}}/\text{cm}^{-1}$): 1623, 1584, 1532, 1465, 1354, 1298, 1253, 1198, 1134, 1083, 1016, 994, 949, 896, 843, 721, 692, 658, 624. ^1H NMR (300.1 MHz, DMSO- d_6): δ 8.02 (d, J = 7.2 Hz, 1H, CH), 7.60–7.10 (m, 11H, 11CH), 6.94 (d, J = 7.9 Hz, 1H, CH), 6.87 (t, J = 7.5 Hz, 1H, CH), 6.67 (s, 1H, CH), 3.63 and 3.61 (2s, 6H, 2OCH₃). ^{13}C NMR (75.1 MHz, DMSO- d_6): δ 153.61, 152.45, 146.11, 141.90, 141.31, 137.99, 131.70, 131.01, 129.66, 129.58, 129.04, 128.77, 127.84, 127.41, 124.15, 121.54, 119.26, 116.94, 115.58, 110.52, 60.42, 56.43. ESI–MS m/z : 536.09 [M]⁺. Anal. Calcd. for C₃₀H₂₂BrN₃O₂: C, 67.17; H, 4.13; N, 7.83.; found: C, 67.28; H, 4.29; N, 8.05%.

α -Glucosidase inhibition assay. α -Glucosidase enzyme (EC3.2.1.20, *Saccharomyces cerevisiae*, 20 U mg⁻¹) and substrate (p-nitrophenyl glucopyranoside) were purchased from Sigma-Aldrich. Enzyme was prepared in potassium phosphate buffer (pH 6.8, 50 mM), as well as substituted benzo[4,5]imidazo[1,2-*c*]quinazoline **6a-c** and highly-substituted imidazo[1,2-*c*]quinazolines **11a-o** were dissolved in DMSO (10% final concentration). The various concentrations of these compounds (20 ml), enzyme solution (20 ml) and potassium phosphate buffer (135 ml) were added in the 96-well plate and incubated at 37 °C for 10 min. Afterwards, the substrate (25 ml, 4 mM) was added to the mentioned mixture and allowed to incubate at 37 °C for 20 min. Finally, the change in absorbance was measured at 405 nm by using spectrophotometer (Gen5, Power wave xs2, BioTek, America). The percentage of enzyme inhibition was calculated using Eq. (6) and IC₅₀ values were obtained from non-linear regression curve using the Logit method.

$$\% \text{ Inhibition} = \left[\frac{(\text{Abs}_{\text{control}} - \text{Abs}_{\text{sample}})}{\text{Abs}_{\text{control}}} \right] \times 100 \quad (6)$$

Kinetic studies. The kinetic analysis was performed for the most potent derivative **11j** to reveal the inhibition mode against α -glucosidase. The 20 ml of enzyme solution (1U ml⁻¹) was incubated with different concentrations (0, 3.1, 6.2, and 12.4 μM) of this compound for 15 min at 30 °C. Afterwards, various concentrations of substrate (p-nitrophenyl glucopyranoside, 1–10 mM) was added to measure the change of absorbance for 20 min at 405 nm by using spectrophotometer (Gen5, Power wave xs2, BioTek, America).

In the presence of a competitive inhibitor, K_m increases while V_{max} does not change. Michaelis–Menten saturation curve for an enzyme reaction shows the relation between the substrate concentration and reaction rate as follow:

$$\frac{v}{V_{\text{max}}} = \frac{[S]}{K_{m_{\text{app}}} + [S]} \quad (7)$$

According to Michaelis–Menten graph, $K_{m_{\text{app}}}$ is also defined as:

$$K_{m_{\text{app}}} = \left(1 + \frac{[I]}{K_I} \right) \quad (8)$$

[I] is the concentration of inhibitor.

Lineweaver Burk plot that provides a useful graphical method for analysis of the Michaelis–Menten is represented as:

$$\frac{1}{V_m} = \frac{K_m}{V_{max}} \left(1 + \frac{[I]}{K_I} \right) \frac{1}{[S]} + \frac{1}{V_{max}} \quad (9)$$

Therefore, the slope of Lineweaver Burk plot is equal to:

$$\text{Slope} = \frac{K_m}{V_{max}} \left(1 + \frac{[I]}{K_I} \right) \quad (10)$$

The $K_{m_{app}}$ value is calculated by Eq. (6):

$$K_{m_{app}} = K_m \left(1 + \frac{[I]}{K_I} \right) \quad (11)$$

Therefore, from replot of $K_{m_{app}}$ Vs. $[I]$, Eq. (7) can be used for the calculation of K_I ^{59,60}:

$$K_{m_{app}} = K_m + \frac{K_m}{K_I} [I] \quad (12)$$

Fluorescence spectroscopy measurements. This assay was carried out for the most potent derivative **11j** to measure the fluorescence intensity. To this aim, different solutions containing different concentrations (0 to 1.0 μM) of the inhibitor and α -glucosidase (3 ml, 0.1 U ml^{-1}) were held for 10 min to equilibrate before measurements. Moreover, the fluorescence of the buffer containing compound **11j** in the absence of the enzyme were subtracted as the background fluorescence. Afterwards, at the excitation wavelength of 280 nm, the fluorescence emission spectra were measured from 300 to 450 nm using a Synergy HTX multi-mode reader (Biotek Instruments, Winooski, VT, USA) equipped with a 1.0 cm quartz cell holder⁶¹.

Molecular docking studies. Molecular docking study using AutoDock4 and Auto Dock Tools (version 1.5.6) was performed on compounds **11a–o** and **6a–c** to elucidate the patterns of their interactions in the active site of the human acid- α -glucosidase (PDB ID: 5NN8). Receptor was prepared by removing water molecules and computing Kollman charges with BIOVIA Discovery Studio visualizer and Auto Dock Tools. To validate the docking procedure, redocking process was performed with acarbose as standard ligand, and RMSD value of 1.57 was achieved. The redocked ligand identified similar binding pose to original co-crystallized position downloaded from RCSB database (5NN8). Acarbose was extracted from the PDB file using BIOVIA Discovery Studio visualizer and saved as a separate PDB file. A possible grid box was determined using Auto Dock Tools (version 1.5.6). Furthermore, genetic algorithm was selected as the searching parameter. This procedure was carried out for different potential grid coordinates. Finally, the best grid coordinates were determined by comparing RMSD values.

Afterwards, ligands **11** and **6** were prepared by adding Gasteiger Charges using Auto Dock Tools, and the docking procedure was conducted with 100 genetic algorithm runs using AutoDock4 and AutoGrid4. The interactions were visualized by PLIP online service⁶² and PyMOL Molecular Graphics System, Version 2.5.2 Schrödinger, LLC.

Statistical analysis. Statistical analysis for all compounds **6a–c** and **11a–o** was performed using SigmaPlot version 14 (Systat-Software, USA). The experiments were replicated three times under the same conditions. Data for each compound was used as mean \pm SD in T test method. A p-value lower than 0.05 was regarded as indicative of statistical significance.

Data availability

The authors confirm that the data supporting the finding of this study are available within the manuscript and supplementary file.

Received: 29 May 2023; Accepted: 12 September 2023

Published online: 21 September 2023

References:

1. Sun, H. *et al.* IDF Diabetes Atlas: Global, regional and country-level diabetes prevalence estimates for 2021 and projections for 2045. *Diabetes Res. Clin. Pract.* **183**, 109119. <https://doi.org/10.1016/j.diabres.2021.109119> (2022).
2. Kshirsagar, R. P. *et al.* SGLT inhibitors as antidiabetic agents: A comprehensive review. *RSC Adv.* **10**, 1733–1756. <https://doi.org/10.1039/C9RA08706K> (2020).
3. Ojebiyi, A. O. The impacts of pharmacological and other interventions for preventing the onset of diabetes. *Int. J. Diabet. Metab. Disord.* **8**, 268–276 (2023).
4. Rush, T., McGeary, M., Sicignano, N. & Buryk, M. A. A plateau in new onset type 1 diabetes: Incidence of pediatric diabetes in the United States Military Health System. *Pediatr. Diabetes* **19**, 917–922. <https://doi.org/10.1111/pedi.12659> (2018).
5. Zheng, Y., Ley, S. H. & Hu, F. B. Global aetiology and epidemiology of type 2 diabetes mellitus and its complications. *Nat. Rev. Endocrinol.* **14**, 88–98. <https://doi.org/10.1038/nrendo.2017.151> (2018).
6. Dowarah, J. & Singh, V. P. Anti-diabetic drugs recent approaches and advancements. *Bioorg. Med. Chem.* **28**, 115263. <https://doi.org/10.1016/j.bmc.2019.115263> (2020).

7. Gao, X. *et al.* Meta-analysis and critical review on the efficacy and safety of alpha-glucosidase inhibitors in Asian and non-Asian populations. *J. Diabet. Investig.* **9**, 321–331. <https://doi.org/10.1111/jdi.12711> (2018).
8. Ghani, U. Re-exploring promising α -glucosidase inhibitors for potential development into oral anti-diabetic drugs: Finding needle in the haystack. *Eur. J. Med. Chem.* **103**, 133–162. <https://doi.org/10.1016/j.ejmech.2015.08.043> (2015).
9. Garlapati, R. *et al.* Development of α -glucosidase inhibitors by room temperature C-C cross couplings of quinazolinones. *Org. Biomol. Chem.* **11**, 4778–4791. <https://doi.org/10.1039/c3ob40636a> (2013).
10. Gurrarn, V. *et al.* Design, synthesis, and biological evaluation of quinazoline derivatives as α -glucosidase inhibitors. *Med. Chem. Res.* **24**, 2227–2237. <https://doi.org/10.1007/s00044-014-1293-5> (2015).
11. Javaid, K. *et al.* 2-Arylquinazolin-4 (3H)-ones: A new class of α -glucosidase inhibitors. *Bioorg. Med. Chem.* **23**, 7417–7421. <https://doi.org/10.1016/j.bmc.2015.10.038> (2015).
12. Zhang, Y. *et al.* Quinazoline-1-deoxyjirimycin hybrids as high active dual inhibitors of EGFR and α -glucosidase. *Bioorg. Med. Chem. Lett.* **27**, 4309–4313. <https://doi.org/10.1016/j.bmcl.2017.08.035> (2017).
13. Wei, M. *et al.* Quinazolinone derivatives: Synthesis and comparison of inhibitory mechanisms on α -glucosidase. *Bioorg. Med. Chem.* **25**, 1303–1308. <https://doi.org/10.1016/j.bmc.2016.09.042> (2017).
14. El-Sayed, N. N. *et al.* Synthesis and evaluation of anticancer, antiphospholipases, antiproteases, and antimetabolic syndrome activities of some 3 H-quinazolin-4-one derivatives. *J. Enzyme Inhib. Med. Chem.* **34**, 672–683. <https://doi.org/10.1080/14756366.2019.1574780> (2019).
15. Santos-Ballardo, L. *et al.* Synthesis, biological evaluation and molecular docking of 3-substituted quinazoline-2, 4 (1 H, 3 H)-diones. *J. Chem. Sci.* **132**, 1–10. <https://doi.org/10.1007/s12039-020-01813-1> (2020).
16. Babatunde, O. *et al.* Dihydroquinazolin-4 (1 H)-one derivatives as novel and potential leads for diabetic management. *Mol. Divers.* **2021**, 1–20. <https://doi.org/10.1007/s11030-021-10196-5> (2021).
17. Tokali, F. S. *et al.* Design, synthesis, molecular docking, and some metabolic enzyme inhibition properties of novel quinazolinone derivatives. *Arch. Pharm.* **354**, 2000455. <https://doi.org/10.1002/ardp.202000455> (2021).
18. Wali, H. *et al.* Synthesis, in vitro, and in silico studies of newly functionalized quinazolinone analogs for the identification of potent α -glucosidase inhibitors. *J. Iran. Chem. Soc.* **18**, 2017–2034. <https://doi.org/10.1007/s13738-021-02159-2> (2021).
19. Ayan, E. K., Soyer, Z. & Uysal, Ş. Synthesis and enzymological characterization of some 2-(substitutedphenylamino) quinazolin-4 (3H)-one derivatives as potent α -glucosidase inhibitors in vitro. *Lett. Drug Des. Discov.* **18**, 723–732. <https://doi.org/10.2174/1570180818999201224121929> (2021).
20. Moheb, M. *et al.* Synthesis and bioactivities evaluation of quinazolin-4 (3H)-one derivatives as α -glucosidase inhibitors. *BMC Chem.* **16**, 1–12. <https://doi.org/10.1186/s13065-022-00885-z> (2022).
21. Sinan Tokali, F. Novel benzoic acid derivatives bearing quinazolin-4 (3H)-one Ring: Synthesis, characterization, and inhibition effects on α -glucosidase and α -amylase. *ChemistrySelect* **7**, e202204019. <https://doi.org/10.1002/slct.202204019> (2022).
22. Ibrahim, A., Sakr, H. M., Ayyad, R. R. & Khalifa, M. M. Design, synthesis, in-vivo anti-diabetic activity, in-vitro α -glucosidase inhibitory activity and molecular docking studies of some quinazolinone derivatives. *ChemistrySelect* **7**, e202104590. <https://doi.org/10.1002/slct.202104590> (2022).
23. Satyanarayana, N. *et al.* Synthesis of 2-styryl-quinazoline and 3-styryl-quinoxaline based sulfonate esters via sp³ C-H activation and their evaluation for α -glucosidase inhibition. *New J. Chem.* **46**, 5162–5170. <https://doi.org/10.1039/D1NJ05644A> (2022).
24. Khalifa, M. M., Sakr, H. M., Ibrahim, A., Mansour, A. M. & Ayyad, R. R. Design and synthesis of new benzylidene-quinazolinone hybrids as potential anti-diabetic agents: In vitro α -glucosidase inhibition, and docking studies. *J. Mol. Struct.* **1250**, 131768. <https://doi.org/10.1016/j.molstruc.2021.131768> (2022).
25. Yar, M. *et al.* Organocatalyzed solvent free an efficient novel synthesis of 2, 4, 5-trisubstituted imidazoles for α -glucosidase inhibition to treat diabetes. *Bioorg. Chem.* **58**, 65–71. <https://doi.org/10.1016/j.bioorg.2014.11.006> (2015).
26. Arshad, T. *et al.* Syntheses, in vitro evaluation and molecular docking studies of 5-bromo-2-aryl benzimidazoles as α -glucosidase inhibitors. *Med. Chem. Res.* **25**, 2058–2069. <https://doi.org/10.1007/s00044-016-1614-y> (2016).
27. Taha, M. *et al.* Synthesis, α -glucosidase inhibitory, cytotoxicity and docking studies of 2-aryl-7-methylbenzimidazoles. *Bioorg. Chem.* **65**, 100–109. <https://doi.org/10.1016/j.bioorg.2016.02.004> (2016).
28. Arshad, T. *et al.* 5-Bromo-2-aryl benzimidazole derivatives as non-cytotoxic potential dual inhibitors of α -glucosidase and urease enzymes. *Bioorg. Chem.* **72**, 21–31. <https://doi.org/10.1016/j.bioorg.2017.03.007> (2017).
29. Zawawi, N. K. N. A. *et al.* Synthesis, molecular docking studies of hybrid benzimidazole as α -glucosidase inhibitor. *Bioorg. Chem.* **70**, 184–191. <https://doi.org/10.1016/j.bioorg.2016.12.009> (2017).
30. Özil, M., Parlak, C. & Baltaş, N. A simple and efficient synthesis of benzimidazoles containing piperazine or morpholine skeleton at C-6 position as glucosidase inhibitors with antioxidant activity. *Bioorg. Chem.* **76**, 468–477. <https://doi.org/10.1016/j.bioorg.2017.12.019> (2018).
31. Rahim, F. *et al.* Synthesis, in vitro α -glucosidase inhibitory potential of benzimidazole bearing bis-Schiff bases and their molecular docking study. *Bioorg. Chem.* **94**, 103394. <https://doi.org/10.1016/j.bioorg.2019.103394> (2020).
32. Aroua, L. M. *et al.* A facile approach synthesis of benzoylaryl benzimidazole as potential α -amylase and α -glucosidase inhibitor with antioxidant activity. *Bioorg. Chem.* **114**, 105073. <https://doi.org/10.1016/j.bioorg.2021.105073> (2021).
33. Mohammadi-Khanaposhtani, M. *et al.* Synthesis, in vitro and in silico enzymatic inhibition assays, and toxicity evaluations of new 4, 5-diphenylimidazole-N-phenylacetamide derivatives as potent α -glucosidase inhibitors. *Med. Chem. Res.* **30**, 1273–1283. <https://doi.org/10.1007/s00044-021-02734-5> (2021).
34. Li, Y. *et al.* Discovery of new 2-phenyl-1H-benzo [d] imidazole core-based potent α -glucosidase inhibitors: Synthesis, kinetic study, molecular docking, and in vivo anti-hyperglycemic evaluation. *Bioorg. Chem.* **117**, 105423. <https://doi.org/10.1016/j.bioorg.2021.105423> (2021).
35. Hasan, H. A., Salman, A. & Abdulmalek, E. Anticancer activity and high content screening of new 6-substituted-5, 6-dihydrobenzo [4, 5] imidazo [1, 2-c] quinazoline derivatives. *Res. J. Pharm. Technol.* **14**, 2397–2405. <https://doi.org/10.52711/0974-360X.2021.00423> (2021).
36. Jadhavar, P. S. *et al.* Benzimidazoquinazolines as new potent anti-TB chemotypes: Design, synthesis, and biological evaluation. *Bioorg. Chem.* **99**, 103774. <https://doi.org/10.1016/j.bioorg.2020.103774> (2020).
37. Li, J.-C. *et al.* Design, synthesis and antifungal activity evaluation of isocryptolepine derivatives. *Bioorg. Chem.* **92**, 103266. <https://doi.org/10.1016/j.bioorg.2019.103266> (2019).
38. Hasan, H. A. *et al.* Synthesis of novel 6-substituted-5, 6-Dihydrobenzo [4, 5] Imidazo [1, 2-c] quinazoline compounds and evaluation of their properties. *J. Mol. Struct.* **1193**, 482–494. <https://doi.org/10.1016/j.molstruc.2019.04.111> (2019).
39. Hasan, H. A. *et al.* Microwave synthesis, crystal structure, antioxidant, and antimicrobial study of new 6-heptyl-5, 6-dihydrobenzo [4, 5] imidazo [1, 2-c] quinazoline compound. *Chem. Cent. J.* **12**, 1–15. <https://doi.org/10.1016/j.molstruc.2019.04.111> (2018).
40. Domány, G. *et al.* Imidazo [1, 2-c] quinazolines with lipid peroxidation inhibitory effect. *Eur. J. Med. Chem.* **33**, 181–187. [https://doi.org/10.1016/S0223-5234\(98\)80007-X](https://doi.org/10.1016/S0223-5234(98)80007-X) (1998).
41. Firozpour, L. *et al.* Design, synthesis and α -glucosidase inhibition study of novel pyridazin-based derivatives. *Med. Chem. Res.* **32**, 713–722. <https://doi.org/10.1007/s00044-023-03027-9> (2023).
42. Sadat-Ebrahimi, S. E. *et al.* Design, synthesis, and biological evaluation of new indole-acrylamide-1, 2, 3-triazole derivatives as potential α -glucosidase inhibitors. *Polycyclic Aromat. Compd.* **42**, 3157–3165. <https://doi.org/10.1080/10406638.2020.1854323> (2022).

43. Peytam, F. *et al.* Design, synthesis, molecular docking, and in vitro α -glucosidase inhibitory activities of novel 3-amino-2, 4-dialylbenzo [4, 5] imidazo [1, 2-a] pyrimidines against yeast and rat α -glucosidase. *Sci. Rep.* **11**, 11911. <https://doi.org/10.1038/s41598-021-91473-z> (2021).
44. Moghimi, S. *et al.* Synthesis, in-vitro evaluation, molecular docking, and kinetic studies of pyridazine-triazole hybrid system as novel α -glucosidase inhibitors. *Bioorg. Chem.* **109**, 104670. <https://doi.org/10.1016/j.bioorg.2021.104670> (2021).
45. Peytam, F. *et al.* An efficient and targeted synthetic approach towards new highly substituted 6-amino-pyrazolo [1, 5-a] pyrimidines with α -glucosidase inhibitory activity. *Sci. Rep.* **10**, 2595. <https://doi.org/10.1038/s41598-020-59079-z> (2020).
46. Moghimi, S. *et al.* Design and synthesis of novel pyridazine N-aryl acetamides: In-vitro evaluation of α -glucosidase inhibition, docking, and kinetic studies. *Bioorg. Chem.* **102**, 104071. <https://doi.org/10.1016/j.bioorg.2020.104071> (2020).
47. Mohammadi-Khanaposhtani, M. *et al.* New biscoumarin derivatives as potent α -glucosidase inhibitors: Synthesis, biological evaluation, kinetic analysis, and docking study. *Polycyclic Aromat. Compd.* <https://doi.org/10.1080/10406638.2018.1509359> (2018).
48. Mohammadi-Khanaposhtani, M. *et al.* Benzoylquinazolinone derivatives as new potential antidiabetic agents: α -Glucosidase inhibition, kinetic, and docking studies. *J. Chin. Chem. Soc.* **67**, 856–863. <https://doi.org/10.1002/jccs.201900268> (2020).
49. Nelson, D. L., Lehninger, A. L. & Cox, M. M. *Lehninger Principles of Biochemistry* (Macmillan, 2008).
50. Adler, A. *Methods in Enzymology* Vol. 27 (Academic Press, 1973).
51. Ross, P. D. & Subramanian, S. Thermodynamics of protein association reactions: Forces contributing to stability. *Biochemistry* **20**, 3096–3102. <https://doi.org/10.1021/bi00514a017> (1981).
52. Farhadian, S. *et al.* Insights into the molecular interaction between sucrose and α -chymotrypsin. *Int. J. Biol. Macromol.* **114**, 950–960. <https://doi.org/10.1016/j.ijbiomac.2018.03.143> (2018).
53. Pedrood, K. *et al.* Design, synthesis, and molecular docking studies of diphenylquinoxaline-6-carbohydrazone hybrids as potent α -glucosidase inhibitors. *BMC Chem.* **16**, 1–13. <https://doi.org/10.1186/s13065-022-00848-4> (2022).
54. SwissADME. (2022). <http://www.swissadme.ch/>.
55. Bischoff, H. Pharmacology of alpha-glucosidase inhibition. *Eur. J. Clin. Invest.* **24**, 3–10. <https://doi.org/10.1111/j.1365-2362.1994.tb02249.x> (1994).
56. McIver, L. A. P. C. & Tripp, J. Acarbose. In *StatPearls [Internet]. Treasure Island (FL)* (StatPearls Publishing, 2023). <https://www.ncbi.nlm.nih.gov/books/NBK493214/>. Accessed 21 Sep 2022.
57. Ahr, H. *et al.* Pharmacokinetics of acarbose. Part I: Absorption, concentration in plasma, metabolism and excretion after single administration of [¹⁴C] acarbose to rats, dogs and man. *Arzneimittelforschung* **39**, 1254–1260 (1989).
58. Daina, A., Michielin, O. & Zoete, V. SwissADME: A free web tool to evaluate pharmacokinetics, drug-likeness and medicinal chemistry friendliness of small molecules. *Sci. Rep.* **7**, 42717. <https://doi.org/10.1038/srep42717> (2017).
59. Dixon, M. The determination of enzyme inhibitor constants. *Biochem. J.* **55**, 170. <https://doi.org/10.1042/bj0550170> (1953).
60. Todd, M. J. & Hausinger, R. Competitive inhibitors of Klebsiella aerogenes urease: Mechanisms of interaction with the nickel active site. *J. Biol. Chem.* **264**, 15835–15842. [https://doi.org/10.1016/S0021-9258\(18\)71553-6](https://doi.org/10.1016/S0021-9258(18)71553-6) (1989).
61. Barker, M. K. & Rose, D. R. Specificity of processing α -glucosidase I is guided by the substrate conformation: Crystallographic and in silico studies. *J. Biol. Chem.* **288**, 13563–13574. <https://doi.org/10.1074/jbc.M113.460436> (2013).
62. Adasme, M. F. *et al.* PLIP 2021: Expanding the scope of the protein–ligand interaction profiler to DNA and RNA. *Nucleic Acids Res.* **49**, W530–W534. <https://doi.org/10.1093/nar/gkab294> (2021).

Acknowledgements

This work was supported and funded by Department of Medicinal Chemistry, Faculty of Pharmacy, Tehran University of Medical Sciences, Tehran, Iran; Gran No. 1400-2-104-54840.

Author contributions

A.F. and F.P. designed the study and conducted the experiments. F.P., F.S.H., and M.H. synthesized the targeted compounds. F.P., Z.E., and L.F. wrote the manuscript, analyzed the characterization data, and prepared the Supporting Information File. B.B. and M.S.M. carried out the docking studies and in silico ADME. S.M. and M.A.F. performed the in vitro enzymatic analysis, kinetic study, circular dichroism spectroscopy, fluorescence spectroscopy measurements, and thermodynamic analysis. S.E.S. and M.B.T. revised the manuscript.

Competing interests

The authors declare no competing interests.

Additional information

Supplementary Information The online version contains supplementary material available at <https://doi.org/10.1038/s41598-023-42549-5>.

Correspondence and requests for materials should be addressed to A.F.

Reprints and permissions information is available at www.nature.com/reprints.

Publisher's note Springer Nature remains neutral with regard to jurisdictional claims in published maps and institutional affiliations.



Open Access This article is licensed under a Creative Commons Attribution 4.0 International License, which permits use, sharing, adaptation, distribution and reproduction in any medium or format, as long as you give appropriate credit to the original author(s) and the source, provide a link to the Creative Commons licence, and indicate if changes were made. The images or other third party material in this article are included in the article's Creative Commons licence, unless indicated otherwise in a credit line to the material. If material is not included in the article's Creative Commons licence and your intended use is not permitted by statutory regulation or exceeds the permitted use, you will need to obtain permission directly from the copyright holder. To view a copy of this licence, visit <http://creativecommons.org/licenses/by/4.0/>.

© The Author(s) 2023